SESSION 3

GENERAL ELEMENTS

Session Chairman

O. C. Zienkiewicz

University of Wales
Swansea, United Kingdom

SOME NEW ELEMENTS FOR THE MATRIX DISPLACEMENT METHOD

J. H. Argyris,* K. E. Buck,** D. W. Scharpf,***
H. M. Hilber,**** G. Mareczek,****

Institut fur Statik und Dynamik der Luft-und
Raumfahrtkonstruktionen, Universitat Stuttgart
Imperial College of Science and Technology,
University of London

This paper presents an aperçu of some of the progress in the application of finite element methods to problems of continuum and structural mechanics. Since space was limited, we could not reproduce the theory and applications of an extensive class of new equilibrium elements, and had to restrict the review to pure kinematic models (matrix displacement method). Moreover, in this latter field we can only give a limited survey of the work carried out at the Institute of Statics and Dynamics and the Department of Aeronautical Structures at Imperial College. With few exceptions, we have ignored the basic theory and have reproduced only some characteristic results. Iterative methods of solutions of problems with a large number of unknowns using the conjugate gradient method are discussed in References 20 and 29.

Broadly, the research presented here covers the following fields: a) Application of more refined elements to three-dimensional stress and strain fields; reference to the corresponding two-dimensional developments are not made. b) Application of two highly efficient classes of fully compatible plate elements. c) A new class of elements for shells of arbitrary geometry. d) A generalization and refinement of the analysis of elastro-plastic deformations of Reference 1, including a new iterative method; (References 23 and 24). Here too, we had to omit a discussion of the kinematic hardening effect (Reference 25). e) Some techniques for the analysis of large displacements and strains.

We cannot enter the far reaching evolution of the structural language ASKA (Reference 27), which bears but little connection with the ASKA packet discussed in Reference 1.

---

*Professor, Director
**Group Leader
***Deputy Group Leader
****Scientific Collaborators

SECTION I

THREE-DIMENSIONAL ANALYSIS

1. GENERAL CONSIDERATIONS

The analysis of two and three-dimensional stress and strain fields was discussed at considerable length in a paper at the First Dayton Conference (Reference 1). In the intervening three years significant advances have been achieved in evolving new elements of greater generality and refinement.

In this connection two associated aspects received particular attention. The first concerns a more faithful reproduction of the actual geometry of a structure than is feasible with the original set of elements, which demands, in general, a polygonization or polyhedrization of the system. For some time it has been evident that by ignoring the actual curvature involves, in certain cases, a marked loss of accuracy. The second extension, closely allied to the first one realized in the theory, is the introduction of polynomials of higher order for the displacement fields. Moreover, while in the past, pure kinematic compatibility was aimed at, some of the new elements allow also for continuity in the first derivatives at certain nodal points. This means that stresses and rotations may be taken as continuous at these nodal points if this is physically admissible. No doubt this yields a more accurate stress field, which is also easier to interpret. However, the incorporation of more degrees of freedom than are strictly necessary from the variational formulation of the problem, involves a so-called overcompatibility with a consequent slight increase in the stiffness of the element. Some of the relevant progress in this field is discussed briefly in References 3 to 6.

Broadly speaking, it may be stated that the new elements are based on the application of a number of distinct interpolation techniques for the direct generation of the so-called 'unit' displacement functions. The latter leads to the immediate formation of the elastic stiffness $\mathbf{k}_E$ and may be also used in a simple manner to obtain the geometrical stiffness $\mathbf{k}_G$. For example, we have the wide class of LUMINA elements, which evolve from Lagrange's interpolation technique. These elements have a three-dimensional hexahedronal form, whose six faces are curved in contrast to what is commonly called a hexahedron element (Figure 1). The geometry of the element is fixed through a unique one to one mapping of the physical space $0x^1x^2x^3$ onto a regular cube $|\xi^\nu| \leq 1$ in the $0\xi^1\xi^2\xi^3$ space by Lagrangian interweaving interpolation functions through a selected set of nodal points (Figure 2). A systematic and consistent arrangement of nodal points is achieved by prescribing $(l+1)$, $(m+1)$, $(n+1)$ points

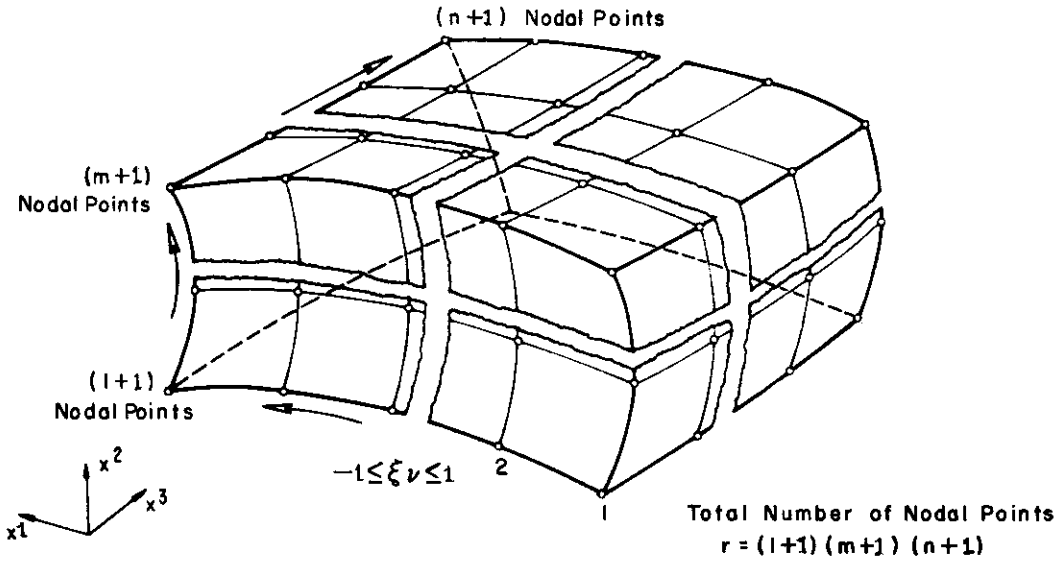

Figure 1. LUMINA - A General Hexahedron Element

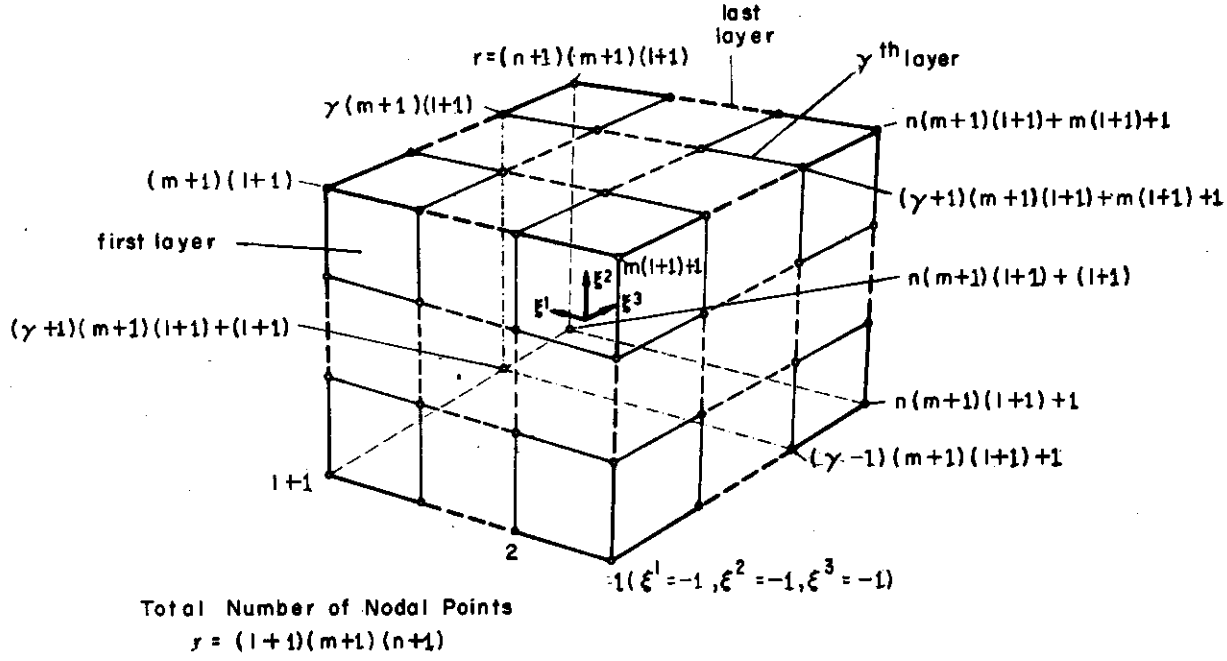

Figure 2. LUMINA - Basic Cube Nodal Point Numbering

in the three curvilinear directions of the actual element. Thus we note that there are in all $r = (l+1)(m+1)$ nodal points. As far as the selection of the fixed set of nodal points is concerned, the reader should consult Reference 3. The order of the Lagrangian interpolation is clearly l, m, n respectively in the basic mapping space. It is evident that these functions are not complete in the ξ space. When $l = m = n$, the elements in question are denoted within ASKA by HEXE r. For an interpolation function of the second order we note that the hexahedronal element has 27 nodal points and 81 unknowns. For a third order interpolation function in all directions we have HEXE 64 with 192 unknowns. These elements are used extensively in the analysis of turbine blades, arch dams and other three-dimensional configurations where the curvature is a decisive factor. It is of interest that HEXE r has a complete displacement field of up to the r^{th} order in the ξ -space.

Another three-dimensional interpolation element in ASKA is called HERMES 8 is discussed in Reference 4. Just as in the LUMINA set, the HERMES element represents a general hexahedronal element with curved faces, and has proved a most useful component block for three-dimensional analysis of complex bodies. The cardinal idea underlying the HERMES development aims at combining the advantages of the Lagrangian and Hermitian interpolation techniques. These may be summarized as follows:

Lagrangian Interpolation Technique. - The geometry of the element is described most easily and systematically by an essential set of nodal points, no derivatives or normal vectors to the surfaces are required.

Hermitian Interpolation Technique. - The derivatives - and hence strain and rotations - enter directly as independent parameters defining the stiffness and other relevant properties of the element. This, if physically admissible, allows one, as stated above, to stipulate continuity of strains and stresses.

It should be expected that, for the same number of freedoms, the resulting strains and stresses generally will be more accurate when using HERMES elements than in the straightforward application of LUMINA elements, where the strains (and hence stresses) are deduced by way of the derivatives of modal Lagrangian functions.

HERMES 8, which is the simplest three-dimensional Hermitian interpolation element, has all its freedoms assigned to the eight corner points, hence any intermediate nodal points necessary for the geometrical shaping of the element, as in LUMINA, do not have any freedoms and are dummy points as far as the kinematic analysis is concerned.

It is evident that HERMES 8 uses a partial set of third order Hermitian polynomials. For all the usefulness and considerable success of the LUMINA and HERMES elements, there is little doubt that, for arbitrary stress fields, it is desirable to apply elements with complete polynomials for the displacement fields. Following Reference 30 this is in practical terms only possible with triangular and tetrahedron elements for two-and three-dimensional stress fields respectively. In the past such elements (see e.g. TRIM 6 and TET 10 of Reference 1) have been evolved allowing up to a linear variation of strains, i.e. a quadratic variation of displacements. In general these proved satisfactory, but the necessity arose to cater for a greater sophistication in the specification of the displacements. This is achieved by the TET 20 and the TEA 8 elements presented in Reference 5. It has been shown in Reference 30 and stated in Reference 2 that third order complete polynomials yielding a second order or parabolic strain distribution fit into a tetrahedron element with 20 nodal points and 60 degrees of freedom, denoted in ASKA as TET 20 Figure 3. The nodal points of this element include, in addition to the four vertices, two points on each edge trisecting the length - a total of twelve points - and four points at the centroids of the faces. The geometrical choice of the edge nodal points and centroids is dictated by symmetry and algebraic convenience. This new element satisfies, of course, kinematic compatibility of the displacements everywhere.

An interesting variant of the use of third order polynomials presents iself, if we stipulate that kinematic compatibility at the four vertices should be extended to all first derivatives of the displacements. The associated degrees of freedom are clearly 4 x 12 = 48. The nodal points of the edges are then redundant, but to satisfy kinematic compatibility of the displacements over the faces of the tetrahedron it is necessary to retain the four 'standard' nodal points at the centroids of the faces of the TET 20, as shown in Figure 4. The total degrees of freedom of such an element - called TEA 8 in ASKA - is clearly 60, as for the TET 20.

It is intriguing to observe that application of the modal technique of Reference 1 leads to a so-called basic or modal stiffness $\mathbf{k}_p$ of the order (60 x 60), from which the stiffness of TET 20 and TEA 8 elements may be derived from two alternative congruent transformations.

Essentially, the technique of Reference 5 is based on the modal idea of Reference 1. However, a more general approach may be achieved by a direct construction of the displacement fields on the basis of a distinct and complete interpolation technique.

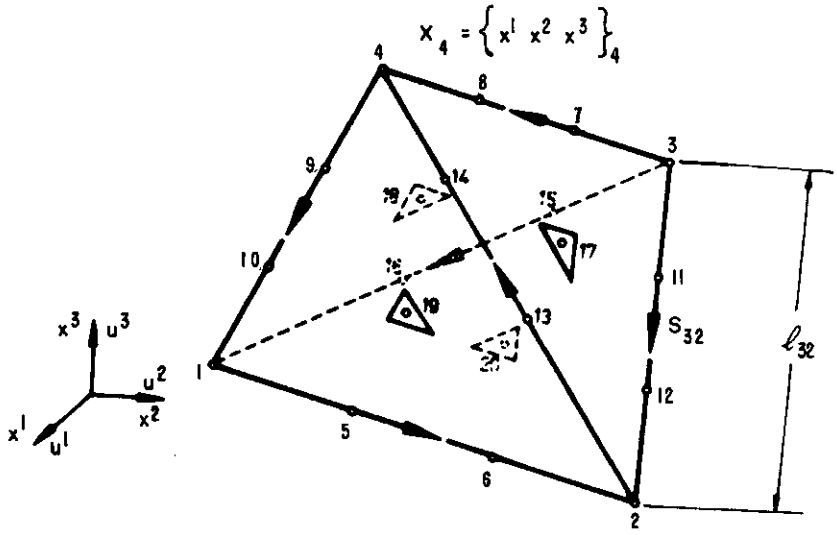

Figure 3. TET 20 Element

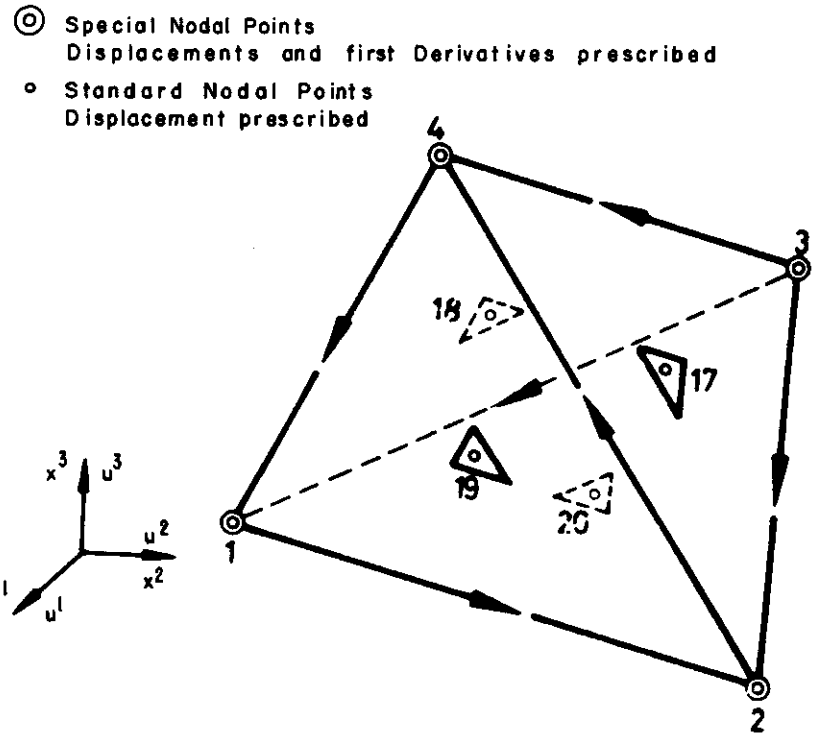

Figure 4. TEA 8 Element

Consider a general TET or TRIM element corresponding to a complete polynomial of m^{th} order. Such a construction is always feasible, as long as the necessary number of internal nodal points f_i are allowed for. We note that

$$f_i = \frac{1}{2}(m+1)(m+2) \qquad \text{for TRIM elements} \qquad (1)$$

$$f_i = \frac{1}{6}(m+1)(m+2)(m+3) \qquad \text{for TET elements} \qquad (2)$$

The modal functions ω, corresponding to unit displacement at one nodal point and zero at all others, may now be determined directly without first establishing a transformation matrix. It is only necessary to assume a regular array of nodal points and apply the complete interpolation scheme in ζ shown in Figure 5. This procedure has been applied within ASKA to TRIM 15, which corresponds to m = 4. Similar techniques may be developed for the corresponding neo-dimensional element groups TRIA and TEA of the order $m \geq 3$. For example, there is the element TRIA 6 for m = 4, which has three 'special' nodal points at the vertices and three 'simpler' ones at the mid-points. where the displacements and their derivatives normal to edges are prescribed; (15 modal functions), cubic variation of strain.

The procedure may also be amplified for $m \geq 2$ to TET and TRIM elements with curved boundaries (edges and faces). It is only necessary to use the same interpolation method of Figure 5, as a one to one mapping device, to construct the actual curvilinear triangular and

The interpolation scheme has as follows:

$$i + j + g + h = m$$

Table of Integer Values:

Co-ord. ν	1	2	3	4
Fixed Integer ℓ	i	j	g	h
Varying Integer L	I	J	G	H

TRIM

TET

The modal function ω^k for point k, fixed by $\zeta_\nu^\ell = \ell/m$ or,

$$\zeta_1^k = i/m, \quad \zeta_2^k = j/m, \quad \zeta_3^k = g/m, \quad \zeta_4^k = h/m$$

is

$$\omega^k = f_1^i \, f_2^j \, f_3^g \, f_4^h$$

Here

$$f_\nu^\ell = c_\nu^\ell \prod_{L=0,\ell=1} (\zeta_\nu - \zeta_\nu^L)$$

and

$$\zeta_\nu^\ell = L/m, \quad c_\nu^\ell = \frac{m^\ell}{\ell!}$$

$\prod_{L=0,\ell-1}$ signifies product of ℓ linear terms in ζ

Figure 5. General TET and TRIM Elements - Complete Interpolation Scheme

tetrahedronal elements from the corresponding basic configurations with straight edges and faces. Such elements are denoted within ASKA by TRIC N and TEC N respectively, N representing the number of nodal points. Moreover, the definition of a geometrical stiffness proves simple now for these elements and the technique may be extended to the large displacement analysis of two- and three-dimensional systems (Reference 6).

2. APPLICATIONS

a. Analysis of an Archdam Using HEXE 64 Elements

The geometry of the archdam analyzed here is shown in Figure 6. The curved surfaces of this system can be approximated best by interpolation elements, such as LUMINA or HERMES. In the present case the idealization uses one layer of 18 curved HEXE 64 elements, the grid of which, projected onto the reference cylinder, is given in Figure 6. The material constants E and ν are taken as 0.20×10^6 kp/cm^2 and 0,15 respectively. A kinematically consistent idealization of the water pressure loading is used in accordance with the deformation modes. The base of the dam is assumed to be built in rigidly with zero displacements at the nodal points. This extreme discretization was adopted at the specifc request of the Civil Engineering Research Council at the Institution of Civil Engineers, Great Britain, for whom this analysis was carried out.

Some typical results of the computations for the air and water face stresses at the plane of symmetry are shown in Figures 7 and 8. On examining, for instance, the radial stresses at the water face, these will be seen to correspond very closely indeed to the applied water pressure, except near the base of the dam, where the effect of the rigid building-in is clearly apparent. These stress peaks can be smoothed out using a foundation model with six additional HEXE's representing the rock bed. For details of this calculation see Reference 7. A corresponding TET 10 analysis of the archdam described here is found in Reference 8, and shows an excellent agreement with the current results.

b. Analysis of a Heated Turbine Vane Using HERMES 8 Elements

The HERMES 8 element has been applied to the analysis of the cylindrical vane with two cooling channels enclosed by solid end parts, as shown in Figure 9. This structure is of considerable complexity not only as far as the geometry is concerned but also with respect to the loading conditions. The temperature varies both in cross-sectional and axial directions, but is symmetrical about the middle cross-section, as is the geometry. Therefore we may

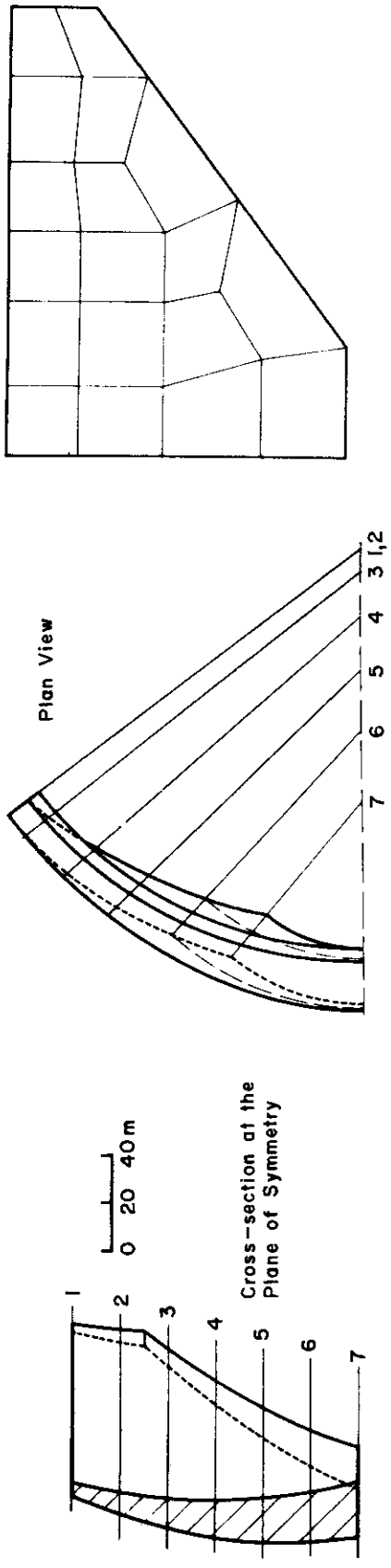

Figure 6. Geometry of Archdam and Grid of HEXE 64 Elements

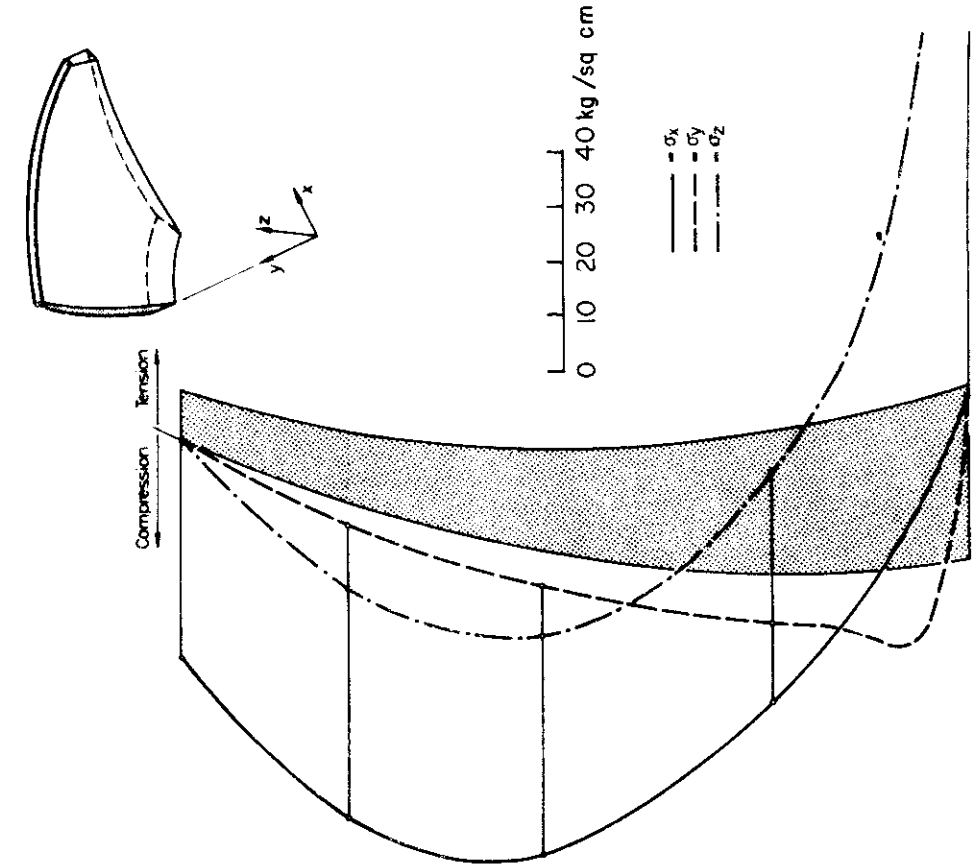

Figure 8. Water Face Stresses at Plane of Symmetry

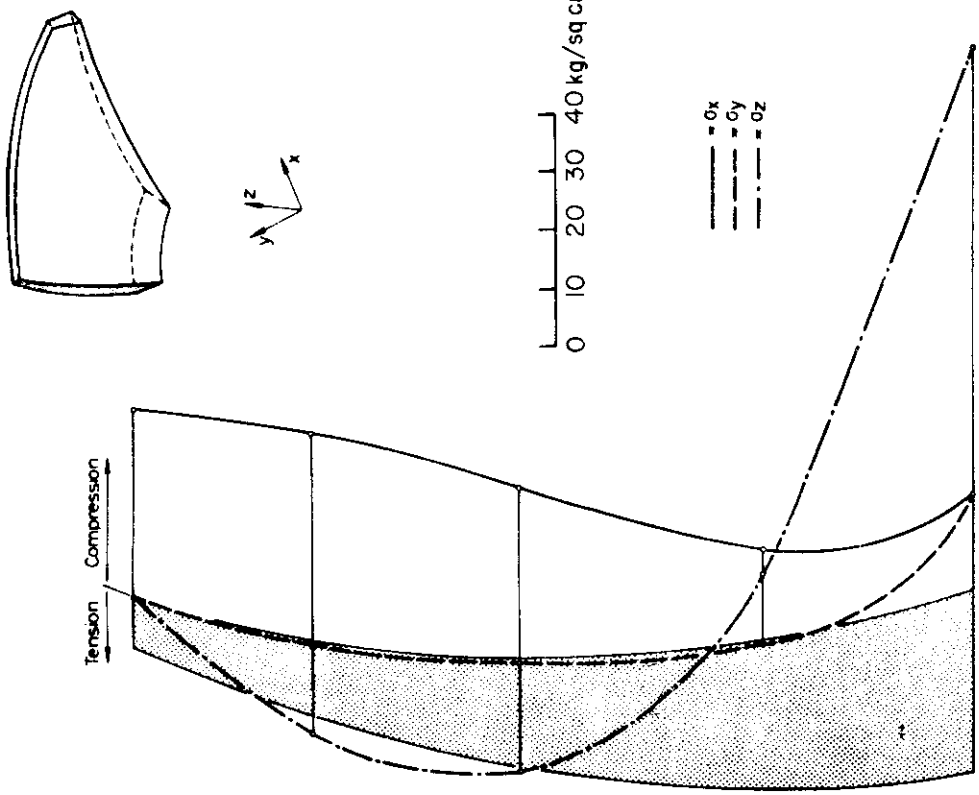

Figure 7. Air Face Stresses at Plane of Symmetry

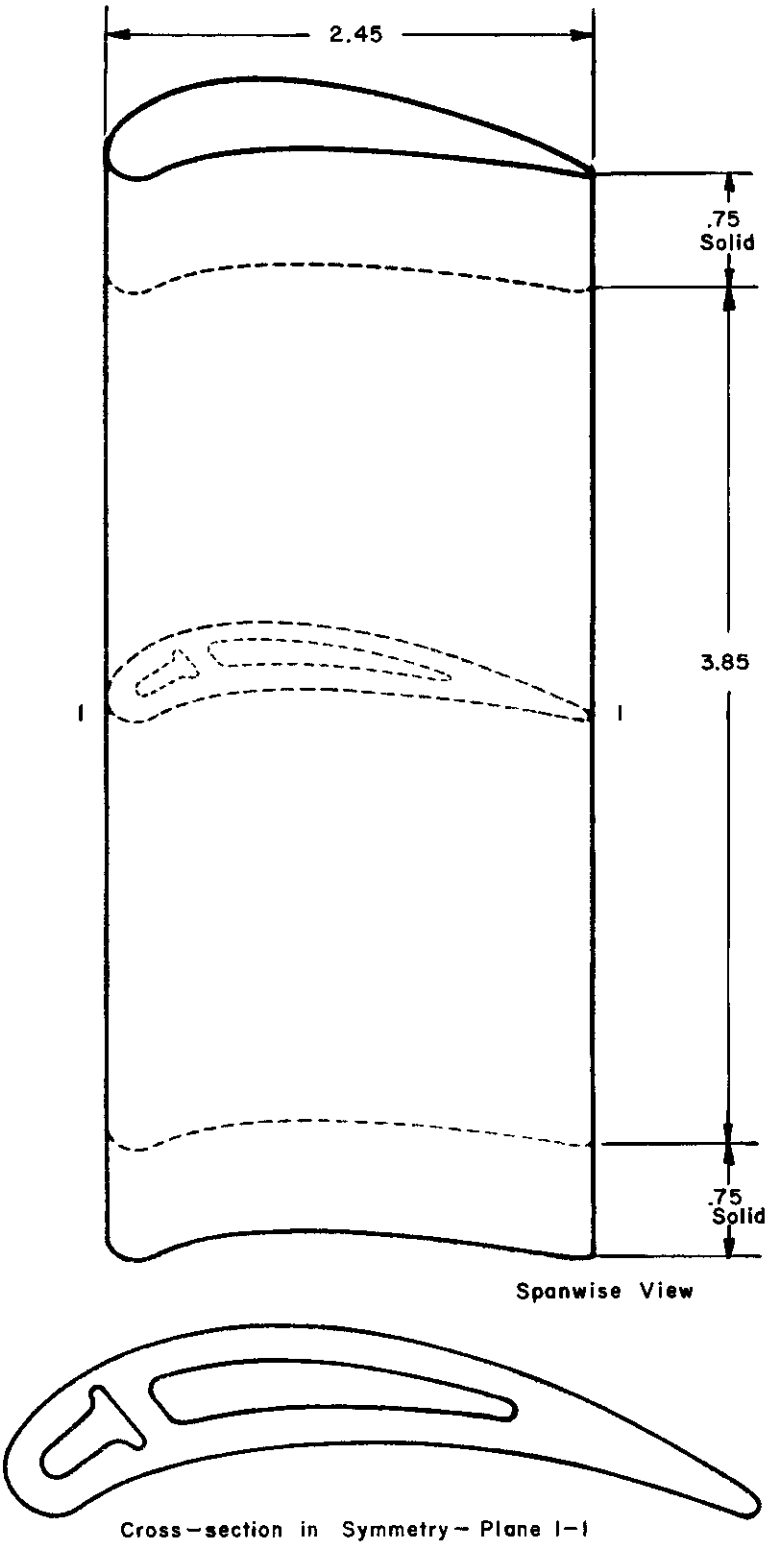

Figure 9. Turbine Vane

only consider half of the system suppressing at the 'root' all displacements orthogonal to the plane of symmetry. Due to the change of temperature within a large range, it is also necessary to allow for variation of the material properties as Young's modulus, Poisson's ratio and thermal coefficients of expansion.

The vane is subdivided into a suitable number of hexahedra with plane surfaces and side length ratios of approximately 1:3:6. The typical middle cross section of the three-dimensional grid is shown in Figures 10 and 11. The question is why not a more general HERMES element, with the desirable feature of curved surfaces? The reason is that the same vane had been calculated previously with six TET 10 elements (Reference 1) in place of one hexahedron (Reference 9). In order to check the agreement between both computations we aimed in changing the geometry as little as possible. To simplify the HERMES 8 idealization a slight modification had, however, to be introduced near the trailing edge (Figure 11). In the TET 10 analysis the material properties are taken as constant within each tetrahedron using a mean temperature, but the thermal strains were allowed to vary linearly. Within a HERMES 8 element Young's modulus and Poisson's ratio as well as the thermal strains are interpolated using the Lagrangian polynomial set of HEXE 27.

It is most interesting to compare the number of elements and unknowns involved in the TET 10 and HERMES 8 discretizations

Number of	TET 10	HERMES 8
Elements	906	155
Nodal points	1770	304 (1825)
Unknowns	5192	3531

Due to the adopted HEXE 27 interpolation scheme the HERMES 8 idealization requires the temperatures, material data, and initial strains at 1825 nodal points. However, kinematic freedoms are only assigned to 304 nodal points. As the 96 degrees of freedom of a HERMES 8 element are concentrated in 8 nodal points, which are common for many adjacent elements, the number of unknowns is remarkably reduced. For lack of space we restrict our presentation to some characteristic results Figures 12 and 13 show a comparison of the spanwise displacement w as calculated with TET 10 and HERMES 8 elements. The distribution of the greatest component stress σ_{zz} is plotted in Figures 14 and 15 for two typical cross sections.

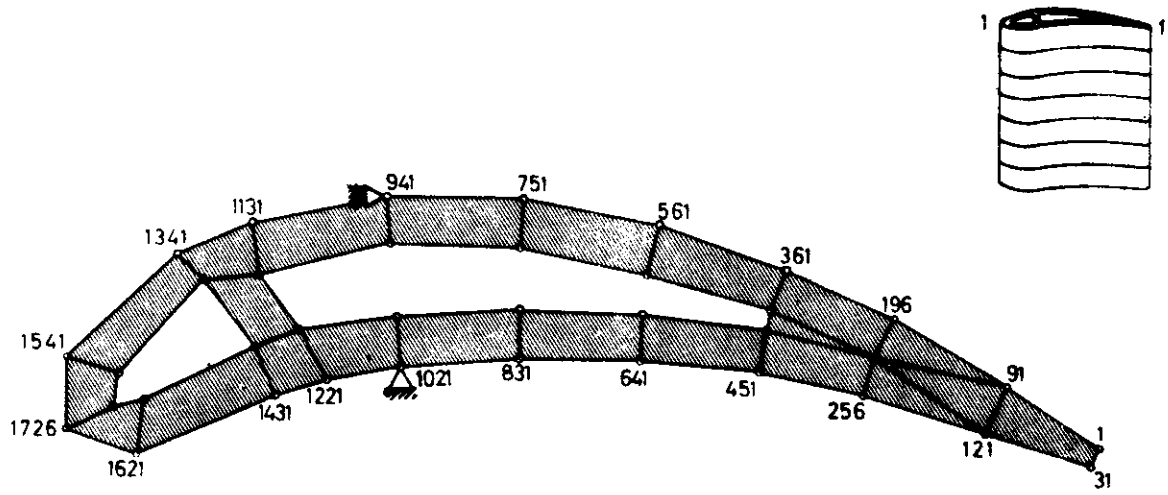

Figure 10. Basic Grid of Elements

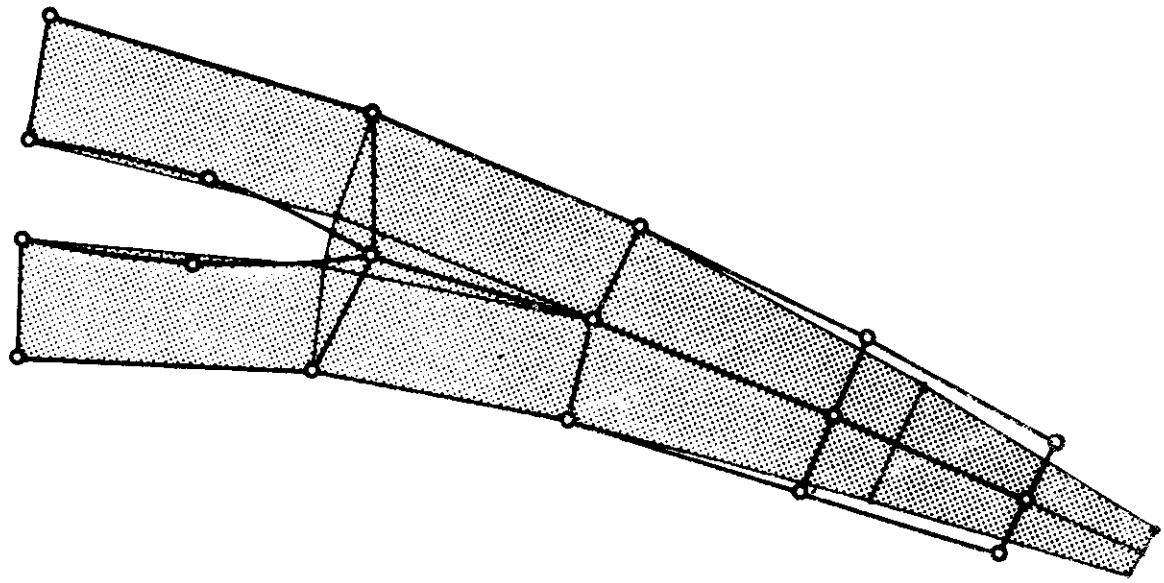

Figure 11. Modification of Grid for HERMES 8 Elements

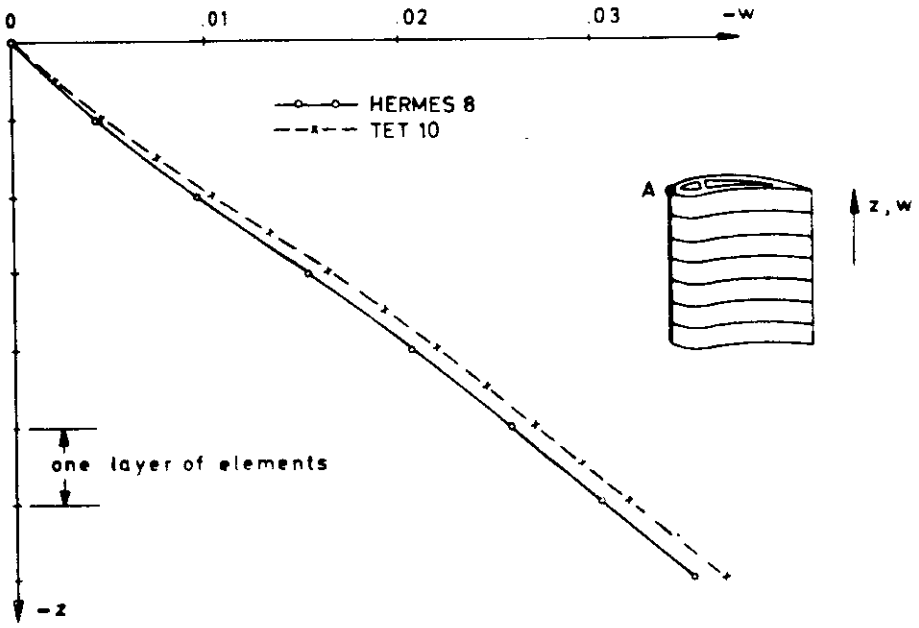

Figure 12. Comparison of Displacement w - TET 10 and HERMES 8 Analyses

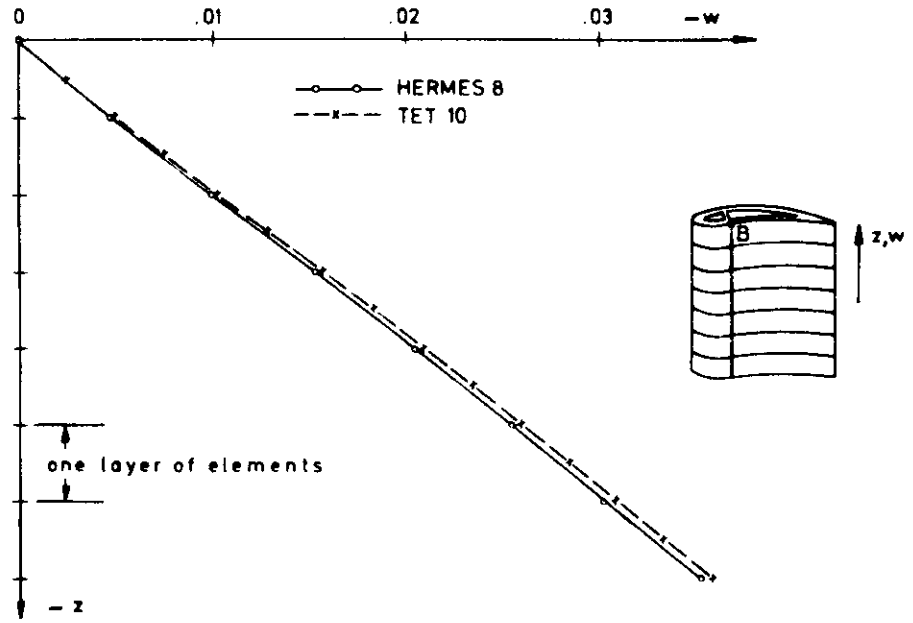

Figure 13. Comparison of Displacement w - TET 10 and HERMES 8 Analyses

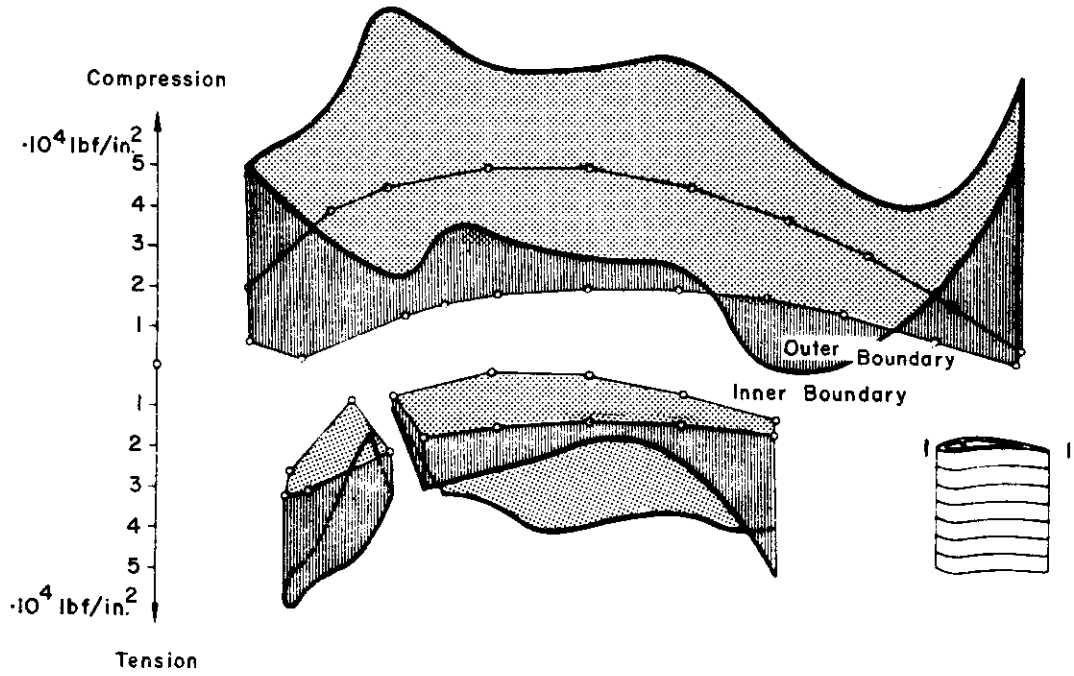

Figure 14. Typical Distribution of Component Stress σ_{zz} in Heated Vane

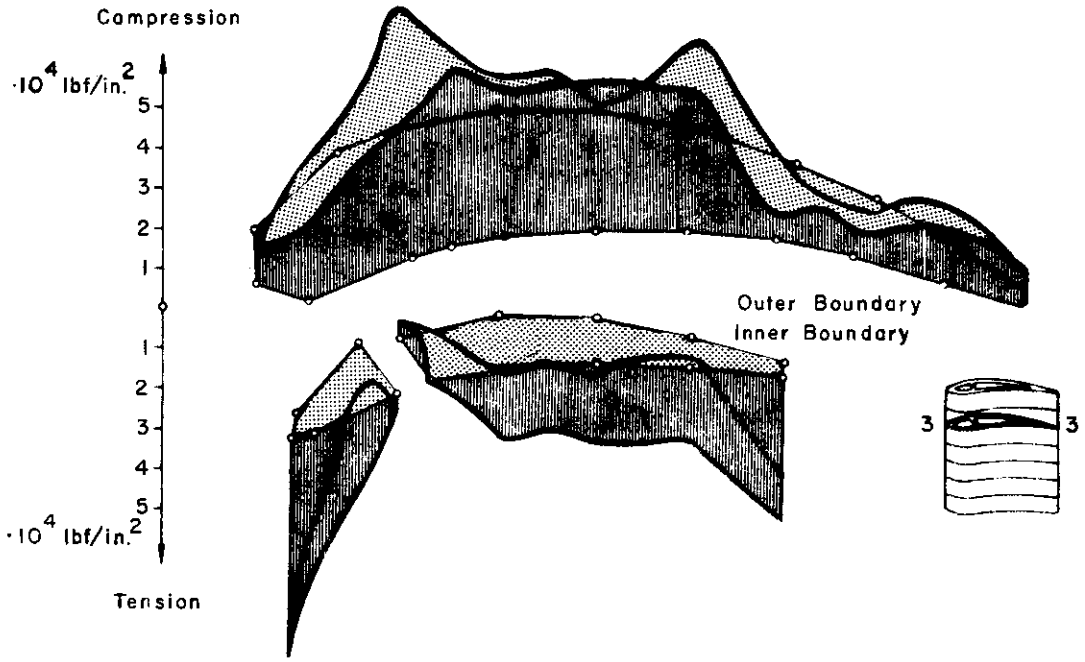

Figure 15. Typical Distribution of Component Stress σ_{zz} in Heated Vane

SECTION II

ANALYSIS OF THIN PLATES

1. GENERAL CONSIDERATIONS

The analytical construction of displacement functions for plate elements subject to bending was discussed at some length in Reference 2. Attention was drawn to both triangular and quadrilateral elements available in the ASKA system, which satisfy either all kinematic compatibility conditions or are deficient in the continuity of the gradient normal to the edge. The most rudimentary elements of the triangular set consist of the so-called fully compatible TRIB 3C, and the TRIB 3 (References 1, and 18), which satisfies the slope condition only at the vertices. The TRIB 3C corresponds in principle, but not in detail, to the element evolved by Bazeley et al (Reference 15), but allows, however, for linear taper. The comments on the pros and cons of these elements were summarized in Reference 2. Note also the interesting construction given by Clough and Tocher (Reference 16) and the elegant solution to the matching of two triangular elements developed by de Veubeke (Reference 17).

It was also pointed out in Reference 2 that a more systematic examination of the fundamental problems arising in triangular elements under bending leads to the conception of a number of distinct families for such elements, which are fully compatible and consistent in their convergence. While, in principle, more sophisticated than TRIB 3C, they are essentially simpler and more accurate in their final formulation. We discuss briefly one particular family known in the ASKA system as the TUBA set.

The TUBA family is based on complete polynomial functions for the deflection w of the order $m \geq 5$. The selection of nodal freedoms, which include at the vertices not only w, and the first derivatives $w_{,x}$, $w_{,y}$ but also all the second derivatives $w_{,xx}$, $w_{,xy}$, $w_{,yy}$, is characteristic. Additional 'simpler' nodal points are strategically placed on the boundary to ensure complete compatibility for w (order m) and the slope normal to the edges $w_{,n}$ (order (m-1)). If necessary, further freedoms f_i are assigned to interior points to define uniquely the s constants

$$s = \frac{1}{2}(m+1)(m+2) \tag{3}$$

of the polynomial or order m. It is easy to confirm that such a scheme

$$f_i = \frac{1}{2}(m-4)(m-5) \tag{4}$$

Thus, for a polynomial of order m = 5, there are no interior points, the corresponding element being called TUBA 6, since, in addition to the three vertices, three nodal points have to be placed in the boundary (Figure 16). For m = 6 we require, in addition to 12 nodal points on the edge, one interior point, the element being denoted by TUBA 13 (Figure 17). The highest order of TUBA element available in ASKA uses m = 7, for which $f_i = 3$, the connotations of the element being TUBA 15 (Figure 18). No practical necessity has arisen until now to expand the TUBA group with higher order functions, although the procedure is straightforward. The number of kinematic freedoms for TUBA 5, 13, 15 is seen to be 21, 28, 36 respectively.

One may, of course, criticize the basic philosophy of these elements for introducing, as freedoms, the three second order derivatives at the vertices, which do not appear, in general, in a variational formulation of the problem, and lead to the aforementioned overconformity. On the other hand, the prescription of the derivatives $w_{,xx}$, $w_{,xy}$, $w_{,yy}$ at the vertices ensures the continuity of moments or stresses there, if this is admissible, which proves valuable from the practical point of view, since it yields accurate estimates of these measures. Moreover, the selected idealization fits neatly into the general concept of the ASKA system. (References 12 and 13) describe the main outline of the theory for the TUBA 6 and TUBA 15 elements. The TUBA set has proved highly efficient in the analysis of plates of arbitrary shapes under static and dynamic loading. This is illustrated by the examples given.

However, for the specific geometry of parallelogram plates, it may be advantageous to use different complete sets in oblique coordinates. To this purpose we have developed PUBA 4, using third order Hermitian polynomials and allowing a complete displacement function of w of the third order. As freedoms we select the w, $w_{,x}$, $w_{,y}$, $w_{,xy}$ at the four nodal points (16 freedoms). Extension to higher order Hermitian interpolation polynomials is evident. The complete theory of PUBA elements is developed in Reference 14; they may be considered as a very broad generalization of the rectangular elements evolved by Bogner, Fox and Schmit (Reference 21). They allow, in addition to arbitrary obliquity, also for arbitrary anisotropy of the material. Of importance is that for both sets of elements the geometrical stiffness k_G for given in-plane membrane loads has been set up. This allows the investigation of instability phenomena in plates.

2. APPLICATIONS

a. The TUBA 6 Element

In order to check the accuracy of the TUBA 6 element we use the classical test example of a simply supported square plate (homogeneous and isotropic, $\nu = 0.3$). Due to the symmetry

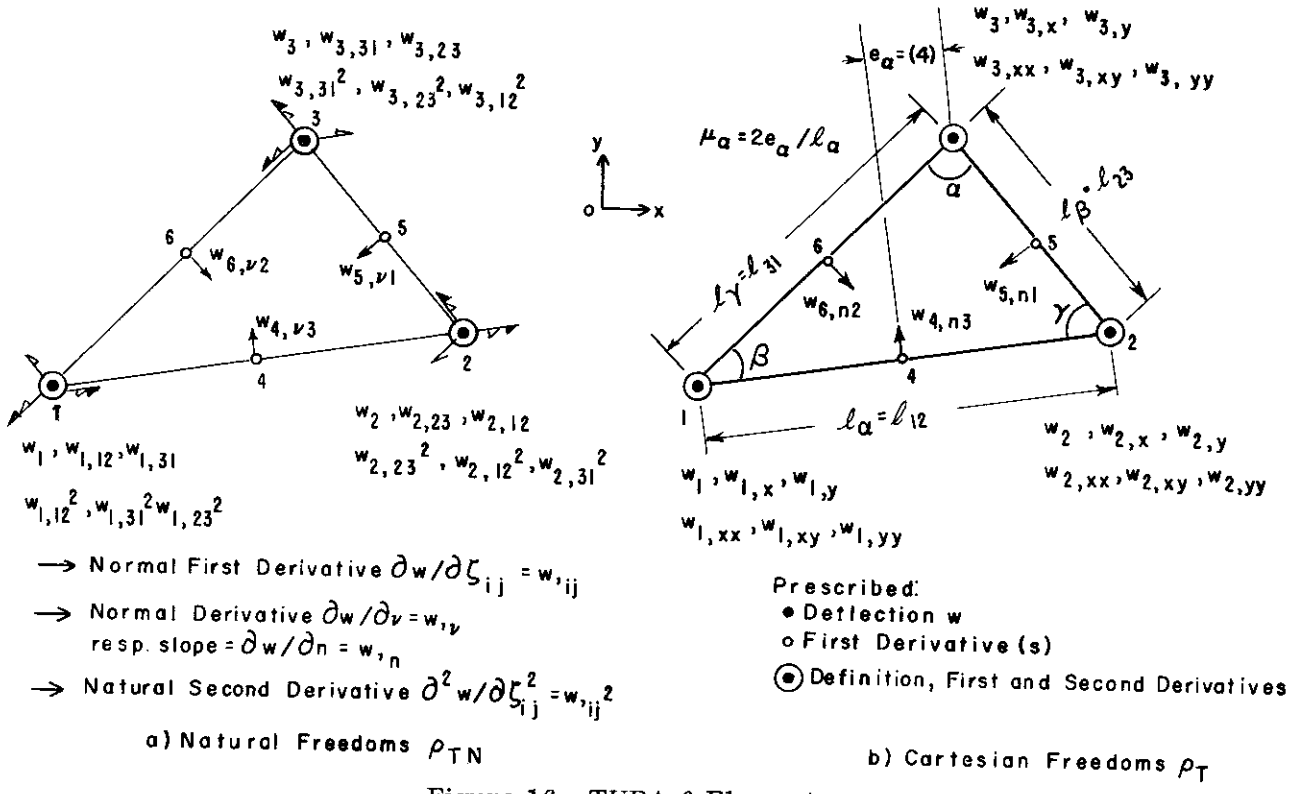

Figure 16. TUBA 6 Element

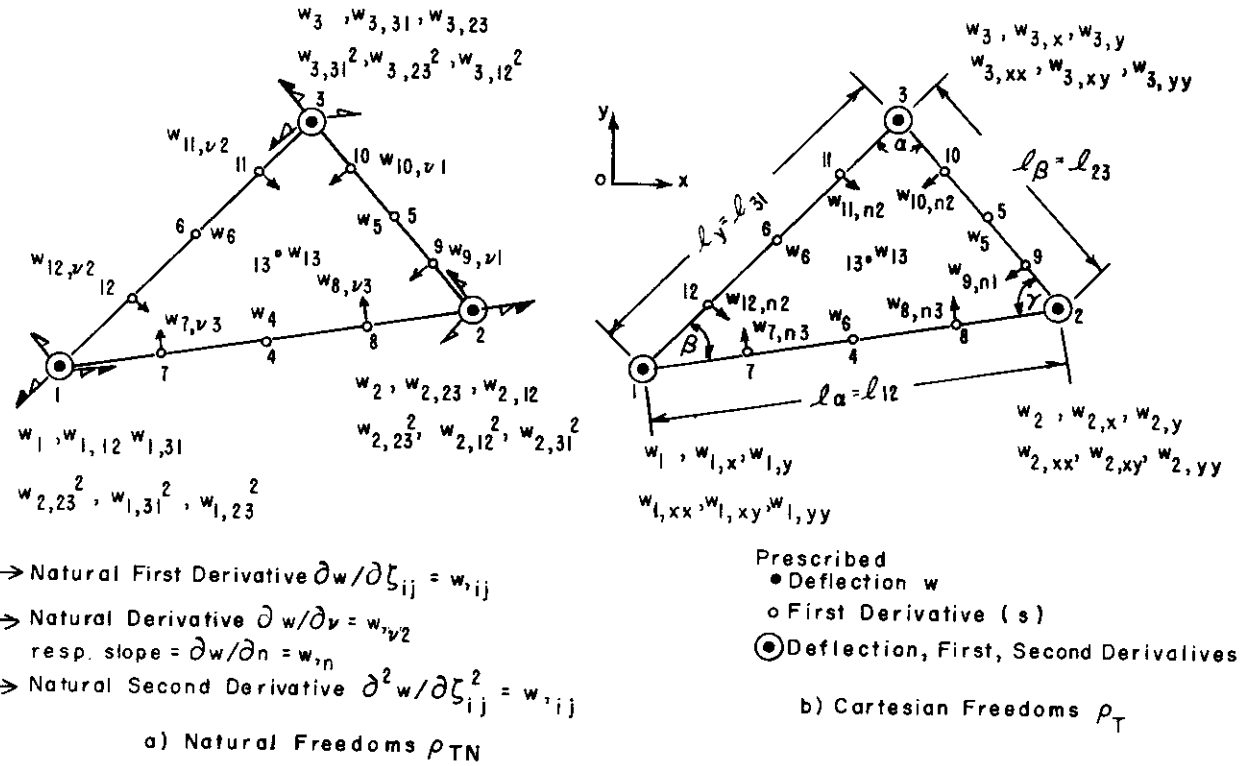

Figure 17. TUBA 13 Element

of the system we may only consider one quarter of the plate; strictly, this could be reduced to one eighth. It is first necessary to introduce the kinematic boundary conditions, e.g. to suppress at a support parallel to a y-axis the freedoms w, $w_{,y}$, $w_{,yy}$. Then, in order to satisfy the dynamic boundary conditions, $w_{,xx}$ is nullified at such a location. Alternatively and equivalently, we may introduce zero moment m_{xx} as an external loading. Two loading cases are analyzed, a concentrated load at the center and a uniform pressure represented by kinematically equivalent loads. The excellent agreement of the finite element results with the exact solution is apparent in Figure 4. Some of the trigonometric series of the analytical theory have been recalculated to a higher accuracy than found in the standard tables in order to have a more reliable yardstick for our computations. The only remarkable deviation is found in the case of the concentrated load for the bending moment at a point B of Figure 19, which lies rather close to the singularity. There is little doubt that TUBA 6 represents the best plate element available to date. We regret that lack of space does not allow any comparison with TUBA 13 and TUBA 15 results.

b. The PUBA 4 Element

A convergence test similar to that of the last section has been undertaken applying PUBA 4 elements for the idealization of a skew plate. For the deflection analysis we consider a plate with a skew angle of 60°; note that the skew angle for a rectangular plate is here 90°. The discretization of the plate proceeds with 4, 8, 12 and 16 elements per side. Kinematically equivalent loads representing a uniform pressure are applied. Following Figure 20 the percentage error in the maximum deflection with respect to the analytical values given by Morley (Reference 37) decreases from + 1.65% to 0.4%, which is quite remarkable. We also analyze the buckling of skew plates subject to an oblique longitudinal stress. In this case it is senseless to draw curves confirming the convergence, because with four elements per side a numerical accuracy of three decimal digits is achieved. We therefore limit the presentation in Figure 21 to the variation of the critical stress versus the skew angle.

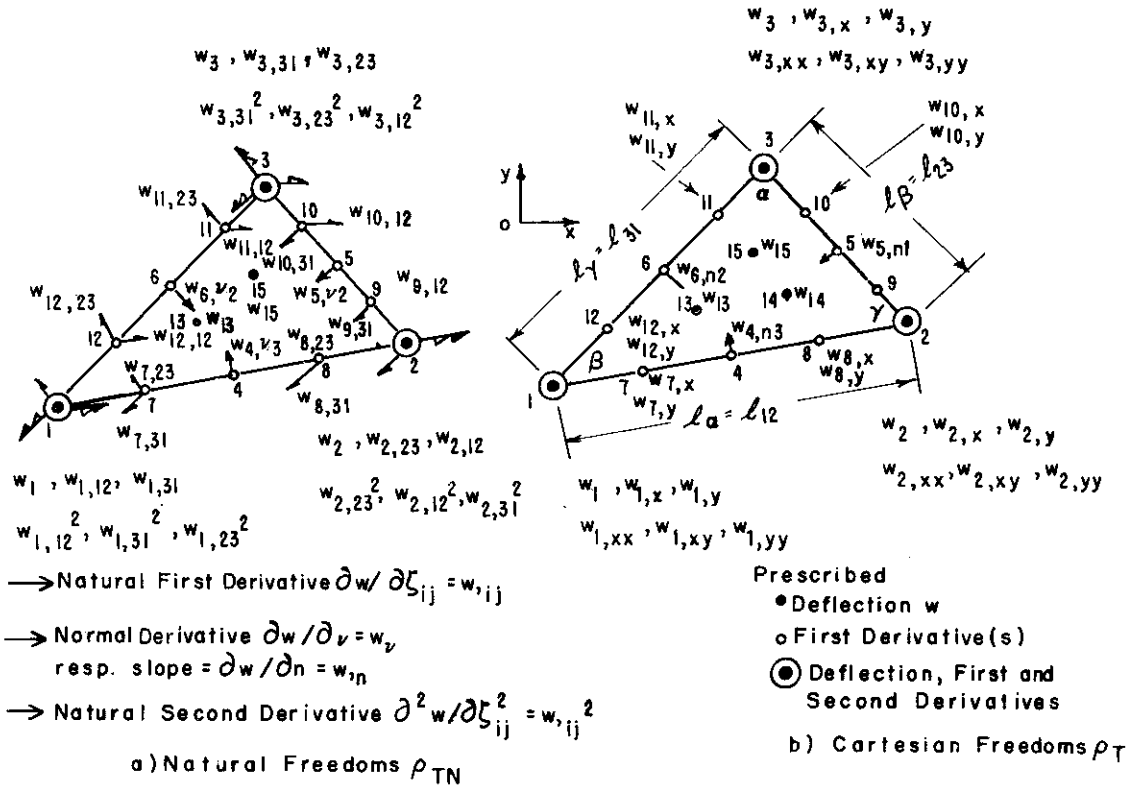

Figure 18. TUBA 15 Element

n	p $\frac{W_{max}}{pa^4/D}$	P $\frac{W_{max}}{Pa^2/D}$
1	0.00405748	0.0113847
2	0.00406230	0.0115486
3	0.00406231	0.0115776
4	0.00406214	0.0115873
Exact	0.00406235	0.0116004

Convergence of Central Deflection

n	p $\frac{M_{max}}{pa^2}$	Point	P $\frac{M_{yy}}{P}$	Point
1	0.0495563	A	—	—
2	0.0479467	A	0.0896	C
3	0.0478986	A	0.1365	B
4	0.0478876	A	0.0984	C
Exact	0.0478864	A	0.1884	B
			0.09868	C

Convergence of Typical Bending Moment

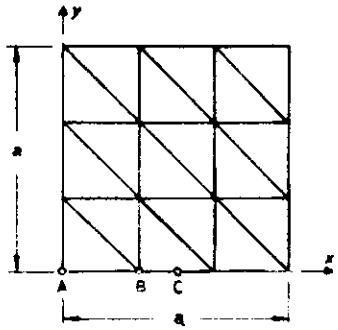

Idealisation of Simply Supported Quadratic Plate

Elements per Half Side: n
(n = 3 shown)

$D = Et^3/12(1-\nu^2)$

Figure 19. Convergence Test for TUBA 6 Element

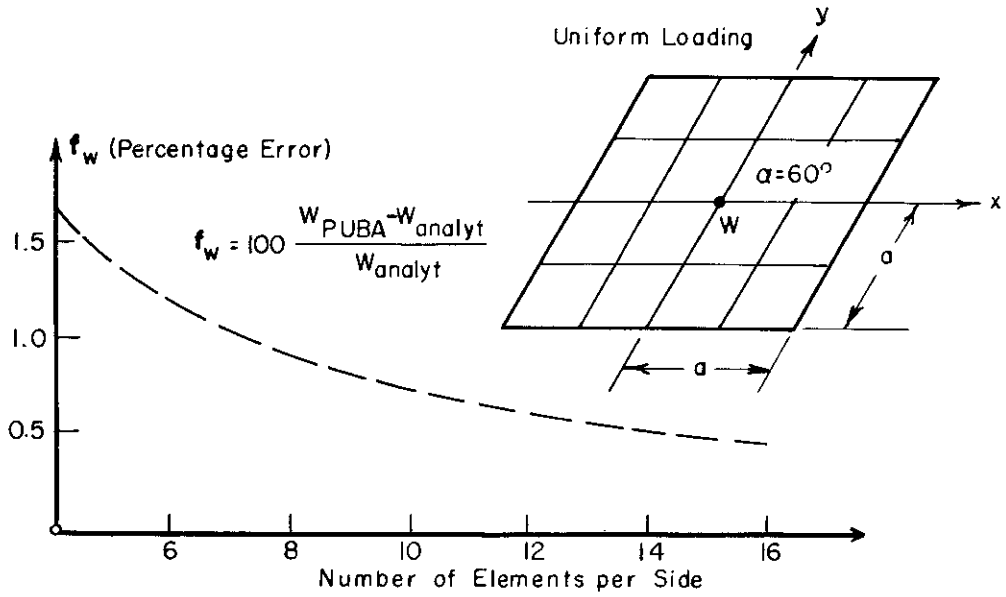

Figure 20. PUBA 4 Element, Convergence of Maximal Deflection of Simply Supported Skew Plate

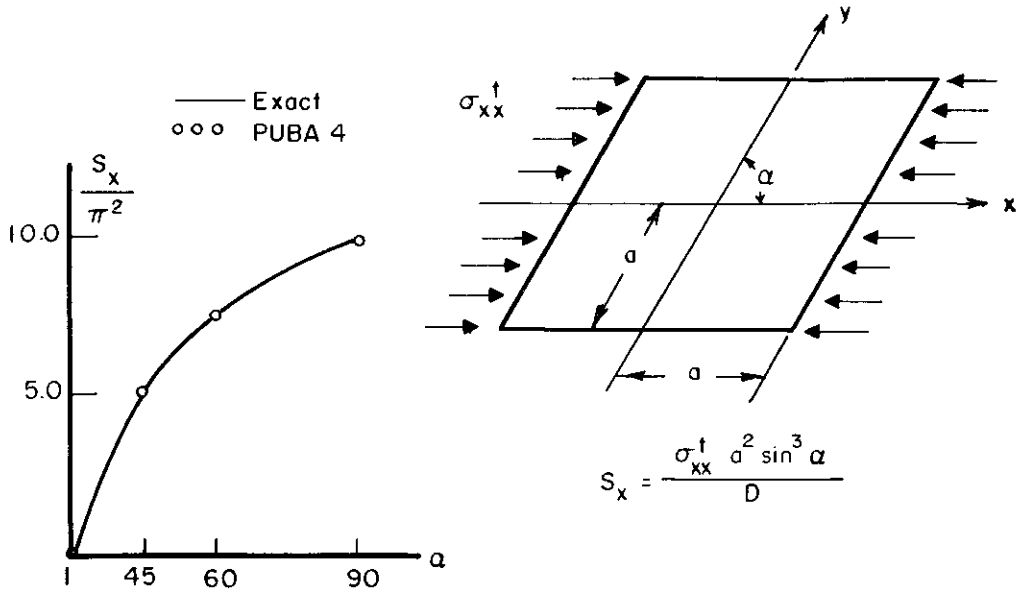

Figure 21. PUBA 4 Element, Critical Stress for a Built-in Plate as Depending on the Skew Angle

SECTION III

THE SHEBA SHELL ELEMENT FOR THE MATRIX DISPLACEMENT METHOD

1. GENERAL CONSIDERATIONS

Considerable effort has been extended over the last years in adapting the matrix displacement method to the specific problems of thin shells under membrane and bending action and developing suitable elements varying in sophistication. Some of the difficulties arising in the process of idealization were reviewed in Reference 2. For example, simple considerations show that a representation of a shell by polyhedron surfaces may lead to serious errors, especially in the presence of pronounced bending and so-called boundary layer effects. For this and other reasons it appears imperative to allow for the curvature of the shell. It is, however, evident, even from a cursory perusal of the literature, that no reliable procedure exists for shells of arbitrary geometry and especially systems with negative Gaussian curvature which are of increasing importance for cooling aggregates and similar systems. Moreover, much of the work developed to date is deficient as far as some basic requirements of the matrix displacement method are concerned. For example, it is well known (Reference 1) that one fundamental prerequisite for establishing reliable stiffness matrices is the existence of true rigid-body motions, giving rise to zero strains. Without this condition the necessary equilibrium of an element may not be satisfied, which may lead to serious errors. It is now well established with the classical work of Reissner (Reference 35), Koiter (Reference 33), and Sanders (References 32 and 34), that Love's formulation of the thin shell theory is deficient since it gives rise to strains under rigid-body rotation unless the shell is spherical. The effect is also nonexistent in shells of revolution under symmetrical loading. The error is, of course, not serious as stressed by Reissner, Koiter and Sanders, as long as the shell is not subjected to pronounced twisting action. Nevertheless, this conclusion applies strictly only to an analysis of a shell as a single system but loses much of its validity when we have to consider a finite element idealization. Here equilibrium has to be satisfied exactly for each element. Moreover, any extension into the realm of large displacements becomes of questionable reliability if this criterion is not satisfied. Any simplifications of the basic theory as expressed, for example, by the shallow shell formulation of Marguerre-Vlassow have also to be viewed critically, when applied to finite elements. This is particularly true when considering kinematic compatibility between adjoining elements.

With this background in mind and with the necessity to provide an element applicable to any geometry and shell configuration we observe once more that the most useful element

must be a triangular one, with curvilinear boundaries and varying curvature. In fact, this should represent a very broad generalization of the TUBA set of Reference 12. It is shown in the present article that interelement compatibility can be achieved, if the three global cartesian displacements are connected to the kinematic freedoms at the nodal points by the same transformation or interpolation procedure as used for the deflection w in the TUBA family (Reference 12). Moreover, in order to ensure zero strains under rigid-body motion it is necessary to develop a mapping of the surface in global cartesian coordinates based on the corresponding set of nodal geometrical data and obeying the same rule of transformation as the displacements. The transformation matrices are expressed most conveniently in terms of the homogeneous triangular coordinates referred to the so-called basic plane triangle formed by the vertices of the element.

One aspect that arises immediately in the initiation of such an investigation is the question whether it is not most convenient to operate with displacements in the directions of the principal curvatures and the normal to the surface, as in the standard shell theory. However, since the mapping of the geometry and the identical one for the displacements is expressed for the cartesian components in terms of the natural homogeneous triangular coordinates of the basic triangle, it is found that the transformations to the directions of principal curvature become extremely complicated and inconvenient, especially as far as the second order derivatives are concerned. It soon becomes evident that it is best to keep within the 'natural' concept originated in Reference 1 and define both membrane strains and curvatures in the directions of the so-called α, β, γ curves corresponding to $\zeta_3, \zeta_1, \zeta_2$ = const. respectively. The theory may now be evolved in a most elegant manner and leads, without any artifices, to a consistent formulation yielding true zero strains under any rigid-body motion. This is truly remarkable in view of the basic simplicity of the analysis. Naturally, our considerations simplify considerably for shell elements of specific geometry such as circular cylindrical shells, shells of revolution and spherical shells.

The general theory is, however, necessary from another point of view. Even for a shell of simplified geometry generality is required once we have to consider large displacements. For example, a careful snap-through investigation of a spherical cap demands an element allowing for varying curvature. Naturally all integrals have to be evaluated numerically, but this presents no problem with a set of suitable pivotal points.

Note that for the adopted idealization the definition of membrane state and corresponding nodal displacements is exactly the same as that for bending in the TUBA element. Thus we

effectively prescribe at the vertices for all displacements not only their values but also their first and second derivatives. In addition the first tangential derivatives normal to the edges are introduced for all displacements at three intermediate points on the edges.

The theory is most easily established by using a judicious combination of vector and matrix calculus. Scalar and vector products appear in this connection and are indicated by the standard symbols; e.g. $\mathbf{a} \cdot \mathbf{b}$ and $\mathbf{a} \times \mathbf{b}$ respectively. Moreover, in order to avoid any misunderstandings the connotation vector is restricted in the present note to true vectors and not applied to column matrices. It should be emphasized, however, that occasionally matrix operations are carried out with actual vectors.

The present work is concerned with thin shells where transverse shear deformations may be ignored. When these become important ASKA uses at present special versions of the LUMINA (Reference 3) and HERMES (Reference 4) sets. Due to lack of space the derivation of the kinematically consistent load and mass matrices, as well as of the geometrical stiffness has to be omitted. These are discussed in Reference 19, together with some other interesting features of the theory.

2. DIFFERENTIAL GEOMETRY OF SURFACES IN HOMOGENEOUS TRIANGULAR COORDINATES

a. Definition of Geometry

Let us assume for the time being that the middle surface of a triangular shell element is defined with respect to a global cartesian system $0x^1x^2x^3$ by the coordinates

$$x^1 = x^1(\zeta_1, \zeta_2, \zeta_3); \quad x^2 = x^2(\zeta_1, \zeta_2, \zeta_3); \quad x^3 = x^3(\zeta_1, \zeta_2, \zeta_3) \tag{4a}$$

which are functions of ζ_i (i = 1, 2, 3), the homogeneous triangular coordinates in the basic triangle 1, 2, 3 (Figures 22 and 23). The functions 4a give a unique mapping of an equilateral triangle with the height 'one' in a Euclidian plane onto the triangular curved middle surface. The position vector to a point on the middle surface may now be written as

$$\mathbf{x} = \left\{ x^1 \; x^2 \; x^3 \right\} = \mathbf{x}(\zeta_1, \zeta_2, \zeta_3) \tag{5}$$

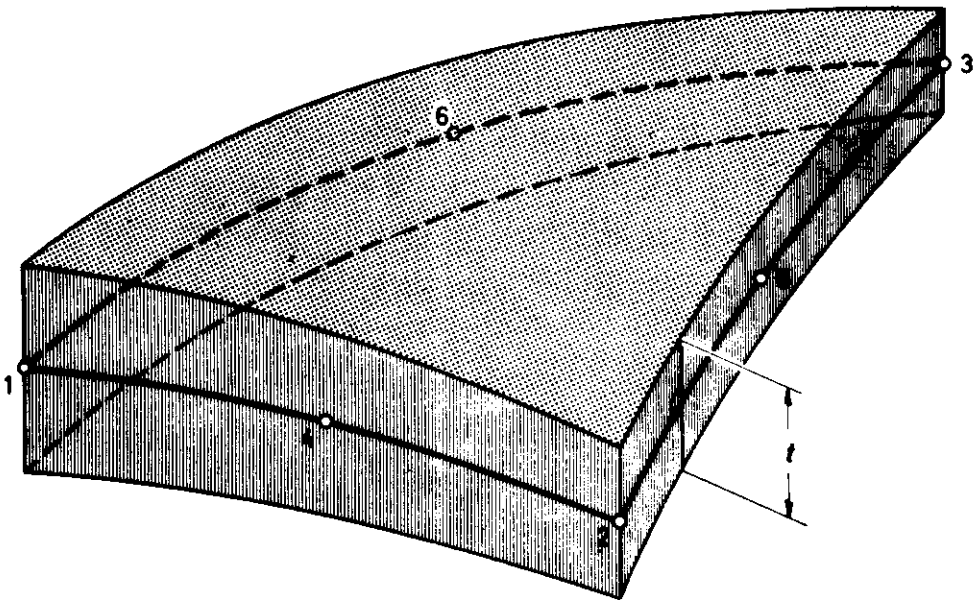

Figure 22. SHEBA 6 Shell Element

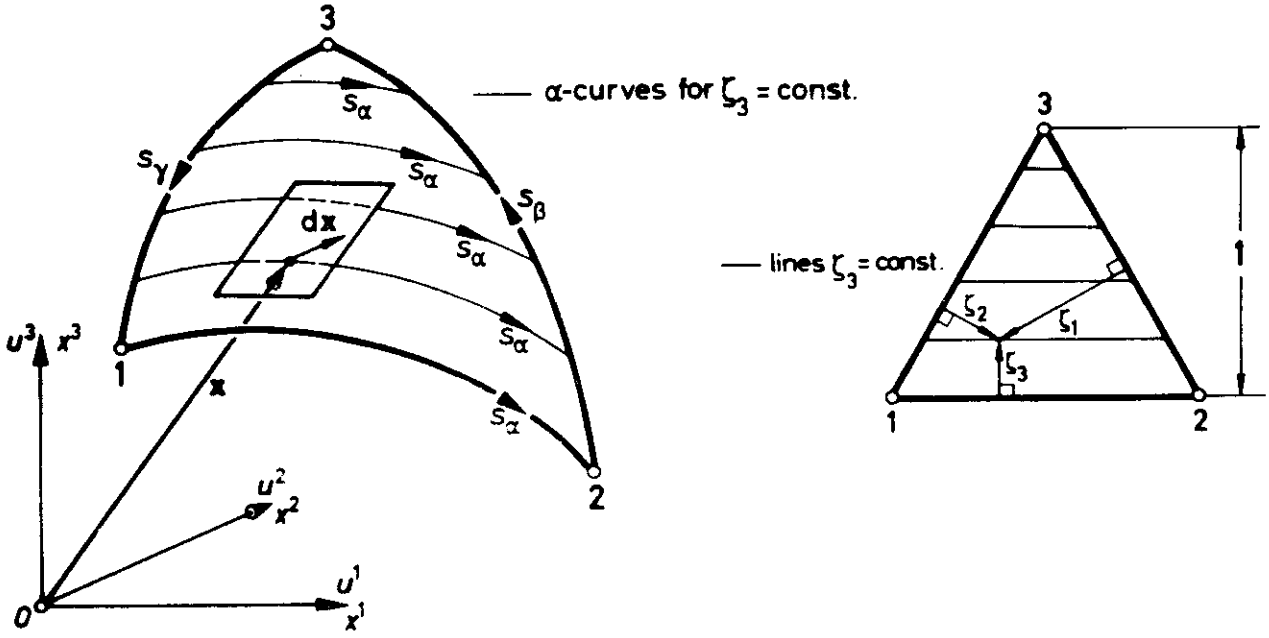

Figure 23. Natural Definition of Middle Surface

b. Metric Relations on the Surface

The incremental vector in the tangential plane is

$$d\mathbf{x} = \mathbf{x}_{,1}\, d\zeta_1 + \mathbf{x}_{,2}\, d\zeta_2 + \mathbf{x}_{,3}\, d\zeta_3 \tag{6}$$

Figure 23, where

$$\mathbf{x}_{,i} = \frac{\partial \mathbf{x}}{\partial \zeta_i} = \left\{ \frac{\partial x^1}{\partial \zeta_i} \quad \frac{\partial x^2}{\partial \zeta_i} \quad \frac{\partial x^3}{\partial \zeta_i} \right\} \tag{7}$$

The incremental arc length ds is obtained from

$$ds^2 = d\mathbf{x} \cdot d\mathbf{x} = d\mathbf{x}^2$$

$$= \mathbf{x}_{,1}^2\, d\zeta_1^2 + \mathbf{x}_{,2}^2\, d\zeta_2^2 + \mathbf{x}_{,3}^2\, d\zeta_3^2 + 2\mathbf{x}_{,1} \cdot \mathbf{x}_{,2}\, d\zeta_1\, d\zeta_2 - 2\mathbf{x}_{,2} \cdot \mathbf{x}_{,3}\, d\zeta_2 d\zeta_3 + 2\mathbf{x}_{,3}\, \mathbf{x}_{,1}\, d\zeta_3\, d\zeta_1 \tag{8}$$

Using the obvious relation

$$d\zeta_1 + d\zeta_2 + d\zeta_3 = 0 \tag{9}$$

one establishes easily the matrix expression

$$\begin{bmatrix} d\zeta_1^2 \\ d\zeta_2^2 \\ d\zeta_3^2 \end{bmatrix} = - \begin{bmatrix} 1 & 0 & 1 \\ 1 & 1 & 0 \\ 0 & 1 & 1 \end{bmatrix} \begin{bmatrix} d\zeta_1\, d\zeta_2 \\ d\zeta_2\, d\zeta_3 \\ d\zeta_3\, d\zeta_1 \end{bmatrix} \tag{10}$$

Applying Equation 10 in Equation 8 we find

$$-ds^2 = (\mathbf{x}_{,2} - \mathbf{x}_{,1})^2\, d\zeta_1\, d\zeta_2 + (\mathbf{x}_{,3} - \mathbf{x}_{,2})^2\, d\zeta_2\, d\zeta_3 + (\mathbf{x}_{,1} - \mathbf{x}_{,3})^2\, d\zeta_3\, d\zeta_1 \tag{11}$$

In what follows we denote a curve on the middle surface as a

α		ζ_3		$d\zeta_3$
β	— curve if	ζ_1	is constant and therefore	$d\zeta_1$ is zero.
γ		ζ_2		$d\zeta_2$

From Equation 11 one verifies that a typical incremental arc length ds_α on an α-curve is given by

$$ds_\alpha^2 = -(\mathbf{x}_{,2} - \mathbf{x}_{,1})^2\, d\zeta_1\, d\zeta_2 \tag{12}$$

Since $dT_3 = 0$ it follows also from Equation 9 that

$$ds_\alpha^2 = (\mathbf{x}_{,2} - \mathbf{x}_{,1})^2\, d\zeta_1^2 = (\mathbf{x}_{,2} - \mathbf{x}_{,1})^2\, d\zeta_2^2 \tag{13}$$

Note that $d\zeta_1$ and $d\zeta_2$ are not independent in Equation 13. We observe that the arc measures on the α, β, γ - curves are now defined by the moduli

$$m_\alpha = \left| \mathbf{x}_{,2} - \mathbf{x}_{,1} \right| \; ; \quad m_\beta = \left| \mathbf{x}_{,3} - \mathbf{x}_{,2} \right| \; ; \quad m_\gamma = \left| \mathbf{x}_{,1} - \mathbf{x}_{,2} \right| \tag{14}$$

c. Natural Derivatives of First Order

Following our usual practice we introduce the operators

$$\frac{\partial}{\partial \zeta_\alpha} = -\frac{\partial}{\partial \zeta_1} + \frac{\partial}{\partial \zeta_2} \; ; \quad \frac{\partial}{\partial \zeta_\beta} = -\frac{\partial}{\partial \zeta_2} + \frac{\partial}{\partial \zeta_3} \; ; \quad \frac{\partial}{\partial \zeta_\gamma} = -\frac{\partial}{\partial \zeta_3} + \frac{\partial}{\partial \zeta_1} \tag{15}$$

As in Reference 12 we also apply the abbreviation

$$\frac{\partial \psi}{\partial \zeta_\mu} = \psi_{,\mu} \tag{16}$$

where μ takes the values α, β, γ and ψ is any vector or scalar function. It follows from Equations 14, 15, and 16 that

$$m_\mu^2 = (\mathbf{x}_{,\mu})^2 \tag{17}$$

We denote as natural derivatives the total derivatives along the α-, β-, γ-curves with respect to the corresponding arc lengths. For a typical μ-curve we have

$$\frac{d}{ds_\mu} = \frac{d\zeta_i}{ds_\mu} \frac{\partial}{\partial \zeta_i} + \frac{d\zeta_j}{ds_\mu} \frac{\partial}{\partial \zeta_j} = \frac{1}{m_\mu} \frac{\partial}{\partial \zeta_\mu} \tag{18}$$

The derivatives $d\zeta_k / ds_\mu$ are obtained from Equation 13 and the signs of the roots are fixed in accordance with the conventions in a plane triangle.

The natural derivatives of the position vector $\mathbf{x}$ are the so-called 'natural' unit vectors

$$\mathbf{e}_\alpha = \frac{d\mathbf{x}}{ds_\alpha} \; , \quad \mathbf{e}_\beta = \frac{d\mathbf{x}}{ds_\beta} \; , \quad \mathbf{e}_\gamma = \frac{d\mathbf{x}}{ds_\gamma} \tag{19}$$

which are lying in the tangential plane to the middle surface; see Figure 24. The normal unit vector to the middle surface is obtained from the three equivalent expressions

$$\mathbf{n} = \frac{\mathbf{e}_\alpha \times \mathbf{e}_\beta}{\left| \mathbf{e}_\alpha \times \mathbf{e}_\beta \right|} = \frac{\mathbf{e}_\beta \times \mathbf{e}_\gamma}{\left| \mathbf{e}_\beta \times \mathbf{e}_\gamma \right|} = \frac{\mathbf{e}_\gamma \times \mathbf{e}_\alpha}{\left| \mathbf{e}_\gamma \times \mathbf{e}_\alpha \right|} \tag{20}$$

Following Figure 24 the moduli in Equation 20 are

$$\left| \mathbf{e}_\alpha \times \mathbf{e}_\beta \right| = \sin\gamma \; ; \quad \left| \mathbf{e}_\beta \times \mathbf{e}_\gamma \right| = \sin\alpha \; ; \quad \left| \mathbf{e}_\gamma \times \mathbf{e}_\alpha \right| = \sin\beta \tag{21}$$

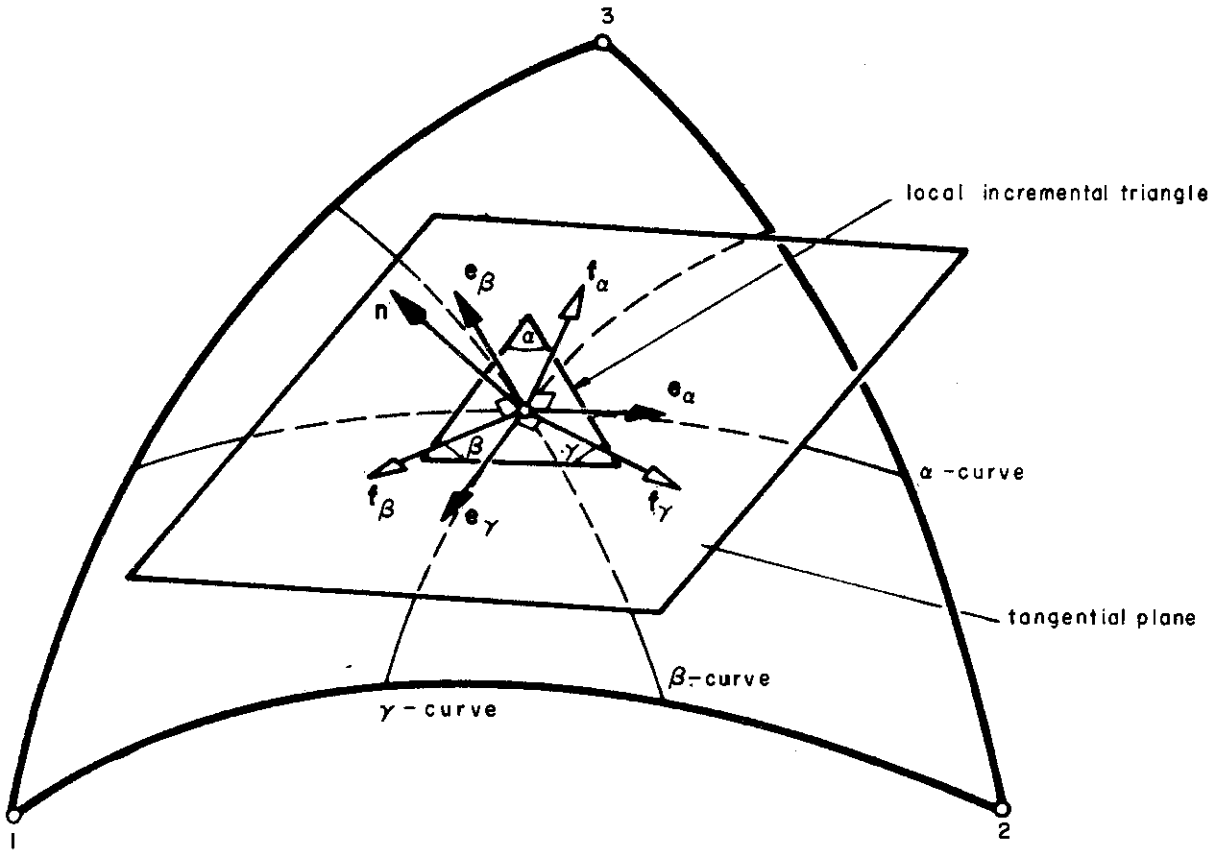

Figure 24. System of Natural Unit Vectors

where α, β, γ are here the angles in a local infinitesimal triangle formed by the α, β, γ curves. The distance along the normal $\mathbf{n}$ is denoted by z. It is occasionally convenient to introduce the unit tangential vectors $\mathbf{f}_\alpha$, $\mathbf{f}_\beta$, $\mathbf{f}_\gamma$ normal to $\mathbf{e}_\alpha$, $\mathbf{e}_\beta$, $\mathbf{e}_\gamma$ respectively and defined by

$$\mathbf{f}_\alpha = \mathbf{n} \times \mathbf{e}_\alpha ; \qquad \mathbf{f}_\beta = \mathbf{n} \times \mathbf{e}_\beta ; \qquad \mathbf{f}_\gamma = \mathbf{n} \times \mathbf{e}_\gamma \tag{22}$$

(see Figure 24). It follows from Equation 15 that

$$\frac{\partial}{\partial \zeta_\alpha} + \frac{\partial}{\partial \zeta_\beta} + \frac{\partial}{\partial \zeta_\gamma} = 0 \tag{23}$$

and hence

$$\mathbf{x}_{,\alpha} + \mathbf{x}_{,\beta} + \mathbf{x}_{,\gamma} = 0 \tag{24}$$

One therefore obtains from Equations 18 and 19 the useful relations

$$m_\alpha \frac{d}{ds_\alpha} + m_\beta \frac{d}{ds_\beta} + m_\gamma \frac{d}{ds_\gamma} = 0 \tag{25}$$

$$m_\alpha \mathbf{e}_\alpha + m_\beta \mathbf{e}_\beta + m_\gamma \mathbf{e}_\gamma = 0 \tag{26}$$

For typographical brevity we sometimes denote the total derivative of a vector $\boldsymbol{\psi}$ with respect to a typical natural arc length s_μ

$$\frac{d\boldsymbol{\psi}}{ds_\mu} = \boldsymbol{\psi}_{,m} \tag{27}$$

When applying this relation to the α, β, γ-curves, m takes in turn the values a, b, c.

d. Natural Derivatives of Second Order

Using Equation 18 one finds

$$\frac{\partial^2}{\partial \zeta_\mu^2} = m_\mu \frac{d}{ds_\mu}\left(m_\mu \frac{d}{ds_\mu}\right) = m_\mu^2 \frac{d^2}{ds_\mu^2} + \frac{dm_\mu}{ds_\mu}\frac{\partial}{\partial \zeta_\mu} \tag{28}$$

We confirm with Equation 17 that

$$\frac{dm_\mu}{ds_\mu} = \frac{1}{m_\mu}\left(\mathbf{e}_\mu \cdot \frac{\partial^2 \mathbf{x}}{\partial \zeta_\mu^2}\right) = \frac{1}{m_\mu}(\mathbf{e}_\mu \cdot \mathbf{x}_{,\mu\mu}) \tag{29}$$

Equation 28 yields now

$$\frac{d^2}{ds_\mu^2} = \frac{1}{m_\mu^2}\left[\frac{\partial^2}{\partial \zeta_\mu^2} - \frac{1}{m_\mu}(\mathbf{e}_\mu \cdot \mathbf{x}_{,\mu\mu})\frac{\partial}{\partial \zeta_\mu}\right] \tag{30}$$

Application of Operator 30 on $\mathbf{x}$ and use of an evident extension of the Convention 27 to second derivatives leads to

$$\frac{d^2\mathbf{x}}{ds_\mu^2} = \mathbf{x}_{,mm} = \frac{d\mathbf{e}_\mu}{ds_\mu} = \mathbf{e}_{\mu,m} = \frac{1}{m_\mu^2}\left[\mathbf{x}_{,\mu\mu} - (\mathbf{e}_\mu \cdot \mathbf{x}_{,\mu\mu})\mathbf{e}_\mu\right] \tag{31}$$

Equation 31 shows immediately that

$$\mathbf{e}_\mu \cdot \frac{d\mathbf{e}_\mu}{ds_\mu} = 0 \tag{32}$$

which follows also from $\mathbf{e}_\mu^2 = 1$. Similarly one obtains from $\mathbf{n}^2 = 1$ and $\mathbf{n} \cdot \mathbf{e}_\mu = 0$

$$\mathbf{n} \cdot \frac{d\mathbf{n}}{ds_\mu} = 0 \quad \text{and} \quad \mathbf{n} \cdot \frac{d\mathbf{e}_\mu}{ds_\mu} = -\frac{d\mathbf{n}}{ds_\mu} \cdot \mathbf{e}_\mu \tag{33}$$

In accordance with the differential geometry of surfaces the radius of curvature in a normal plane $\mathbf{n} - \mathbf{e}_\mu$ is given by

$$\frac{1}{R_{\mu\mu}} = \frac{d\mathbf{n}}{ds_\mu} \cdot \mathbf{e}_\mu = -\mathbf{n} \cdot \mathbf{x}_{,mm} = -\frac{1}{m_\mu^2}\, \mathbf{n} \cdot \mathbf{x}_{,\mu\mu} \tag{34}$$

e. Variation of an Element of Arc Length with z

Figure 25 shows that the position vector $\mathbf{x}'$ to a point at a normal distance z from the middle surface is

$$\mathbf{x}' = \mathbf{x} + z\ \mathbf{n} \tag{35}$$

Let us write the incremental tangential vector $d\mathbf{x}_\mu$ between two points $\mathbf{x}_1$ and $\mathbf{x}_2$ on the middle surface as

$$d\mathbf{x}_\mu = \mathbf{x}_2 - \mathbf{x}_1 = \mathbf{e}_\mu\ ds_\mu \tag{36}$$

Then $d\mathbf{x}'_\mu$ in a parallel surface at a distance z is

$$d\mathbf{x}'_\mu = \mathbf{x}'_2 - \mathbf{x}'_1 = (\mathbf{x}_2 + z\mathbf{n}_2) - (\mathbf{x}_1 + z\mathbf{n}_1) = d\mathbf{x}_\mu + z\frac{d\mathbf{n}}{ds_\mu} ds_\mu = (\mathbf{e}_\mu + z\frac{d\mathbf{n}}{ds_\mu}) ds_\mu \tag{37}$$

where the differential form arises from Taylor's expansion. Neglecting terms of higher order one obtains

$$(d\mathbf{x}'_\mu)^2 = (ds'_\mu)^2 = (1 + 2z\mathbf{e}_\mu \cdot \frac{d\mathbf{n}}{ds_\mu})(ds_\mu)^2 \tag{38}$$

or to a first approximation

$$ds'_\mu = (1 + z\mathbf{e}_\mu \cdot \frac{d\mathbf{n}}{ds_\mu})\, ds_\mu \tag{39}$$

f. Element of Area

To establish a theory of thin shells we have to consider here only an element of area $d\Omega$ on the middle surface. On a α-curve we have e.g. an incremental tangential vector

$$d\mathbf{x}_\alpha = \mathbf{x}_{,1}\, d\zeta_1 + \mathbf{x}_{,2}\, d\zeta_2 = (\mathbf{x}_{,2} - \mathbf{x}_{,1})\, d\zeta_2 = \mathbf{x}_{,\alpha}\ d\zeta_2 \tag{40}$$

and similarly on β- and γ-curves

$$d\mathbf{x}_\beta = \mathbf{x}_{,\beta}\ d\zeta_3\ ; d\mathbf{x}_\gamma = \mathbf{x}_{,\gamma}\ d\zeta_1 \tag{41}$$

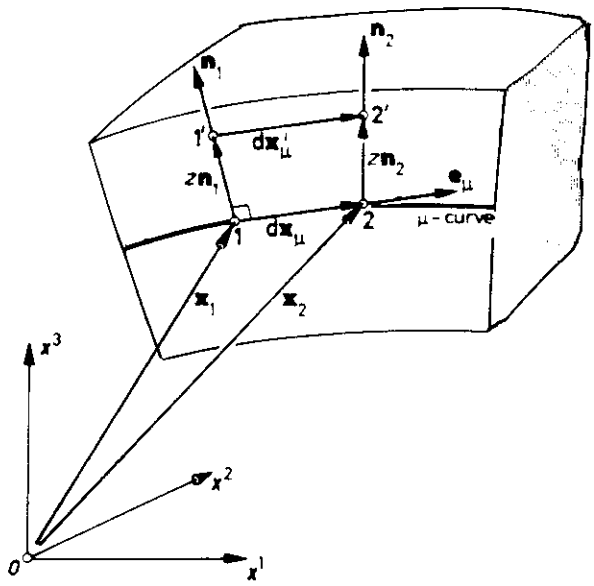

Figure 25. Dependence of Arc Length on z

Now $d\Omega$ may be written as

$$d\Omega = \left| dx_\alpha \times dx_\beta \right| = \left| dx_\beta \times dx_\gamma \right| = \left| dx_\gamma \times dx_\alpha \right|$$

$$= \left| x_{,\alpha} \times x_{,\beta} \right| d\zeta_2\, d\zeta_3 = \left| x_{,\beta} \times x_{,\gamma} \right| d\zeta_3\, d\zeta_1 = \left| x_{,\gamma} \times x_{,\alpha} \right| d\zeta_1\, d\zeta_2 \qquad (42)$$

Forming the vector product of $x_{,\mu}$ with Expression 24 we confirm that

$$S = \left| x_{,\alpha} \times x_{,\beta} \right| = \left| x_{,\beta} \times x_{,\gamma} \right| = \left| x_{,\gamma} \times x_{,\alpha} \right| \qquad (43)$$

Using Relations 18, 19, and 21 we find

$$S = m_\alpha\, m_\beta \sin\gamma = m_\beta\, m_\gamma \sin\alpha = m_\gamma\, m_\alpha \sin\beta \qquad (44)$$

3. STRAIN-DISPLACEMENT RELATIONS

a. Definition of Displacements

Let us assume that the global cartesian displacements of the middle surface are given by the functions

$$u^1 = u^1(\zeta_1, \zeta_2, \zeta_3)\ ;\ u^2 = u^2(\zeta_1, \zeta_2, \zeta_3)\ ;\ u^3 = u^3(\zeta_1, \zeta_2, \zeta_3) \qquad (45)$$

We now define the displacement vector of a point in the middle surface as

$$\mathbf{u} = \left\{ u^1 \quad u^2 \quad u^3 \right\} = \mathbf{u}(\zeta_1, \zeta_2, \zeta_3) \tag{46}$$

As mentioned in the introduction it is necessary, in order to develop a consistent theory, to express the geometry and displacements in an identical manner. This is in contrast to standard shell theory which usually operates with displacement components in the principal directions of curvature and in the normal direction to the surface.

b. Natural Membrane Strains

Following Figure 26 we consider a typical element $d\mathbf{x}_\mu$ of a μ-curve between points $\mathbf{x}_1$ and $\mathbf{x}_2$. Using a bar to denote a deformed state we

$$\bar{\mathbf{x}}_1 = \mathbf{x}_1 + \mathbf{u}_1 \quad ; \quad \bar{\mathbf{x}}_2 = \mathbf{x}_2 + \mathbf{u}_2 \tag{47}$$

Following an argument similar to that in "Variation of an Element of Arc Length With z".

$$d\bar{\mathbf{x}}_\mu = \bar{\mathbf{x}}_2 - \bar{\mathbf{x}}_1 = \mathbf{x}_2 - \mathbf{x}_1 + \mathbf{u}_2 - \mathbf{u}_1 = d\mathbf{x}_\mu + \frac{d\mathbf{u}}{ds_\mu} ds_\mu \tag{48}$$

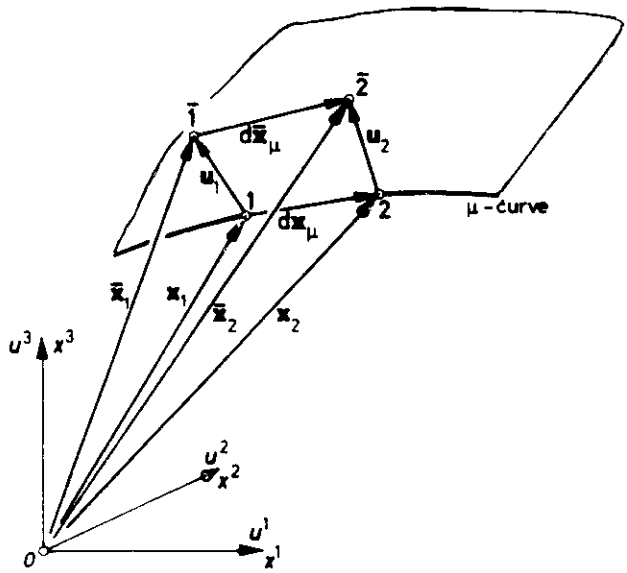

Figure 26. Total Natural Membrane Strain

and therefore

$$d\bar{s}_\mu = (1 + e_\mu \cdot u_{,m}) ds_\mu \tag{49}$$

The total natural strain in the middle surface and the μ-direction is now by definition

$$\epsilon_{\mu o} = \frac{d\bar{s}_\mu - ds_\mu}{ds_\mu} = e_\mu \cdot \frac{du}{ds_\mu} = e_\mu \cdot u_{,m} \tag{50}$$

In the last expressions the shorthand notation $du / ds_\mu = u_{,m}$ of Equation 21 has been applied. The matrix of the natural membrane strains is therefore

$$\epsilon_{No} = \{ \epsilon_{\alpha o} \quad \epsilon_{\beta o} \quad \epsilon_{\gamma o} \} = \{ e_\alpha \cdot u_{,a} \quad e_\beta \cdot u_{,b} \quad e_\gamma \cdot u_{,c} \} \tag{51}$$

Consider next an element dx'_μ at a distance z from the middle surface. If we neglect for the time being the change of the normal due to deformation we observe that the total elongation of the element dx'_μ is the same as that of dx_μ. Since the arc length is z dependent the strain is modified, however, and becomes

$$\epsilon'_{\mu o} = \epsilon_{\mu o} \frac{ds_\mu}{ds'_\mu} = \epsilon_{\mu o} \frac{1}{1 + (z / R_{\mu\mu})} \tag{52}$$

where the last relation follows from Equation 39.

c. Rotation of Natural Bi-peds due to Deformation

Let us consider the displaced 'unit' infinitesimal arc elements in the α- and β-directions. Following Figure 27 we have

$$\bar{e}_\alpha = e_\alpha + \frac{du}{ds_\alpha} \; ; \qquad \bar{e}_\beta = e_\beta + \frac{du}{ds_\beta} \tag{53}$$

The unit normal vector in the deformed state is then

$$\bar{n} = \frac{\bar{e}_\alpha \times \bar{e}_\beta}{| \bar{e}_\alpha \times \bar{e}_\beta |} \tag{54}$$

Applying Equation 53 and neglecting higher order terms in the derivatives of the displacement vector one finds

$$\bar{e}_\alpha \times \bar{e}_\beta = e_\alpha \times e_\beta + e_\alpha \times u_{,b} + u_{,a} \times e_\beta \tag{55}$$

or

$$(\bar{\mathbf{e}}_\alpha \times \bar{\mathbf{e}}_\beta)^2 = (\mathbf{e}_\alpha \times \mathbf{e}_\beta)^2 + 2(\mathbf{e}_\alpha \times \mathbf{e}_\beta)(\mathbf{e}_\alpha \times \mathbf{u}_{,b} + \mathbf{u}_{,a} \times \mathbf{e}_\beta)$$
$$= \sin^2\gamma \left[1 + \frac{2}{\sin\gamma}\, \mathbf{n} \cdot (\mathbf{e}_\alpha \times \mathbf{u}_{,b} + \mathbf{u}_{,a} \times \mathbf{e}_\beta)\right] \tag{56}$$

It follows that

$$\frac{1}{|\bar{\mathbf{e}}_\alpha \times \bar{\mathbf{e}}_\beta|} = \frac{1}{\sin\gamma}\left[1 - \frac{1}{\sin\gamma}\, \mathbf{n} \cdot (\mathbf{e}_\alpha \times \mathbf{u}_{,b} + \mathbf{u}_{,a} \times \mathbf{e}_\beta)\right] \tag{57}$$

Substitution of Equation 57 in Equation 54 and application of Equation 55 yields, after some vector transformations,

$$\mathbf{m} = \bar{\mathbf{n}} - \mathbf{n} = \frac{1}{\sin\gamma}\left[\mathbf{n} \times (\mathbf{e}_\alpha \times \mathbf{u}_{,b} + \mathbf{u}_{,a} \times \mathbf{e}_\beta)\right] \times \mathbf{n} \tag{58}$$

where $\mathbf{m}$ is the change of the unit normal vector. Expression 58 may be interpreted as a rotation of $\mathbf{n}$ through the angular vector Ω_n, i.e.

$$\mathbf{m} = \Omega_n \times \mathbf{n} \tag{59}$$

with

$$\Omega_n = \frac{1}{\sin\gamma}\, \mathbf{n} \times (\mathbf{e}_\alpha \times \mathbf{u}_{,b} + \mathbf{u}_{,a} \times \mathbf{e}_\beta) = \frac{1}{\sin\gamma}\left[(\mathbf{n} \cdot \mathbf{u}_{,b})\mathbf{e}_\alpha - (\mathbf{n} \cdot \mathbf{u}_{,a})\mathbf{e}_\beta\right] \tag{60}$$

Using Relation 25 applied to $\mathbf{u}$ as well as relation 26 it may be readily proved that the following alternative formulations hold for Ω_n

$$\Omega_n = \frac{1}{\sin\gamma}\left[(\mathbf{n} \cdot \mathbf{u}_{,b})\mathbf{e}_\alpha - (\mathbf{n} \cdot \mathbf{u}_{,a})\mathbf{e}_\beta\right] = \frac{1}{\sin\alpha}\left[(\mathbf{n} \cdot \mathbf{u}_{,c})\mathbf{e}_\beta - (\mathbf{n} \cdot \mathbf{u}_{,b})\mathbf{e}_\gamma\right] = \frac{1}{\sin\beta}\left[(\mathbf{n} \cdot \mathbf{u}_{,a})\mathbf{e}_\gamma - (\mathbf{n} \cdot \mathbf{u}_{,c})\mathbf{e}_\alpha\right] \tag{61}$$

To obtain the angular vector of the bi-ped $\mathbf{n} - \mathbf{e}_\mu$ one has to add to Ω_n a rotational vector $\Omega_{\mu n}$ parallel to $\mathbf{n}$ which expresses the missing rotation of $\mathbf{e}_\mu$ about the normal $\mathbf{n}$. Clearly, following Figure 27

$$\Omega_{\mu n} = \left[\mathbf{u}_{,m} \cdot (\mathbf{n} \times \mathbf{e}_\mu)\right] \mathbf{n} = (\mathbf{u}_{,m} \cdot \mathbf{f}_\mu)\, \mathbf{n} \tag{62}$$

The total rotation of the bi-ped $\mathbf{n} - \mathbf{e}_\mu$ is thus

$$\Omega_\mu = \Omega_n + \Omega_{\mu n} \tag{63}$$

d. Natural Bending Strains

Figure 28 shows that the vector $d\mathbf{x}'_\mu$ in a parallel surface at a distance z is transformed due to the rotation vector Ω_μ into

$$d\bar{\mathbf{x}}'_\mu = d\mathbf{x}'_\mu + \Omega_\mu \times d\mathbf{x}'_\mu + z\left(\frac{d\Omega_\mu}{ds_\mu} ds_\mu \times \mathbf{n}_2\right) \tag{64}$$

Since the second and third terms on the right hand side are small quantities $\mathbf{n}_2$ may be replaced by $\mathbf{n}$. We next find, using the identity $d\mathbf{x}'_\mu \cdot (\Omega_\mu \times d\mathbf{x}'_\mu) = 0$

$$(d\bar{\mathbf{x}}'_\mu)^2 = (ds'_\mu)^2 = (ds'_\mu)^2 + 2z\,\mathbf{e}_\mu \cdot \left(\frac{d\Omega_\mu}{ds_\mu} \times \mathbf{n}\right) ds'_\mu\, ds_\mu \tag{65}$$

Hence we deduce

$$d\bar{s}'_\mu = ds'_\mu + z\,\mathbf{e}_\mu \cdot (\Omega_{\mu,m} \times \mathbf{n})\, ds_\mu \tag{66}$$

Defining in the usual manner the measure of bending strain by

$$\chi_\mu = \frac{d\bar{s}'_\mu - ds'_\mu}{z\, ds_\mu} \tag{67}$$

(see also Reference 31), we obtain

$$\chi_\mu = \mathbf{e}_\mu \cdot (\Omega_{\mu,m} \times \mathbf{n}) = \Omega_{\mu,m} \cdot (\mathbf{n} \times \mathbf{e}_\mu) = \Omega_{\mu,m} \cdot \mathbf{f}_\mu \tag{68}$$

For orthogonal coordinates this expression can be compared with Gol'denveizer's (Reference 31) corresponding vector expressions. The actual bending strain at a distance z is therefore given by

$$\epsilon'_\mu = \frac{d\bar{s}'_\mu - ds'_\mu}{ds'_\mu} = \frac{z}{1 + (z/R_{\mu\mu})} \chi_\mu \tag{69}$$

We form the three components $\chi_\alpha, \chi_\beta, \chi_\gamma$ as the column matrix

$$\boldsymbol{\chi}_N = \{\chi_\alpha \quad \chi_\beta \quad \chi_\gamma\} \tag{70}$$

e. Formulae for the Bending Strains

We consider here the typical bending measure χ_α, which is split into two parts

$$\chi_\alpha = \chi_{\alpha n} + \chi_{\alpha\alpha} = \mathbf{n} \cdot \left(\mathbf{e}_\alpha \times \frac{d\Omega_n}{ds_\alpha}\right) + \frac{d\Omega_{\alpha n}}{ds_\alpha} \cdot (\mathbf{n} \times \mathbf{e}_\alpha) \tag{71}$$

Let us first derive $d\Omega_n/ds_\alpha$. From the first formulation of Equation 61 we find

$$\frac{d\Omega_n}{ds_\alpha} = \frac{1}{\sin\gamma}\left\{\frac{d}{ds_\alpha}\left[(n\cdot u_{,b})e_\alpha - (n\cdot u_{,a})e_\beta\right] - \frac{d\sin\gamma}{ds_\alpha}\Omega_n\right\} \tag{72}$$

Writing Expression 21 in the form $\sin\gamma = n\cdot(e_\alpha \times e_\beta)$ we deduce, using the first of Equation 33

$$\frac{d\sin\gamma}{ds_\alpha} = n\cdot\left(\frac{de_\alpha}{ds_\alpha}\times e_\beta + e_\alpha \times \frac{de_\beta}{ds_\alpha}\right) \tag{73}$$

Substitution of Equation 73 into 72 yields a lengthy expression. Carrying out however the vector operations indicated in Equation 71 one finally obtains using the Convention 27 for n, u, e_α

$$\chi_{\alpha n} = -n_{,a}\cdot u_{,a} - n\cdot u_{,aa} + \frac{1}{\sin\gamma}n\cdot\left[(e_{\alpha,a}\cdot f_\alpha)u_{,b} - (e_{\alpha,a}\cdot f_\beta)u_{,a}\right] \tag{74}$$

In order to symmetrize Equation 74 we carry out corresponding operations on the third formula in Equation 61 and form the mean value of the two equivalent expressions to find

$$\chi_{\alpha n} = -n_{,a}\cdot u_{,a} - n\cdot u_{,aa} - \frac{1}{2}\left[e_{\alpha,a}\cdot\left(\frac{1}{\sin\gamma}f_\beta - \frac{1}{\sin\beta}f_\gamma\right)\right](n\cdot u_{,a}) + \frac{1}{2}(e_{\alpha,a}\cdot f_\alpha)\left[n\cdot\left(\frac{1}{\sin\gamma}u_{,b} - \frac{1}{\sin\beta}u_{,c}\right)\right] \tag{75}$$

For the second term $\chi_{\alpha\alpha}$ one readily derives

$$\chi_{\alpha\alpha} = \left[\frac{dn}{ds_\alpha}\cdot(n\times e_\alpha)\right]\left[\frac{du}{ds_\alpha}\cdot(n\times e_\alpha)\right] = (n_{,a}\cdot f_\alpha)(u_{,a}\cdot f_\alpha) \tag{76}$$

Combining $\chi_{\alpha n}$ and $\chi_{\alpha\alpha}$ one finds the relatively simple formula

$$\chi_\alpha = (n\cdot e_{\alpha,a})(e_\alpha\cdot u_{,a}) - n\cdot u_{,aa} - \frac{1}{2}\left[e_{\alpha,a}\cdot\left(\frac{1}{\sin\gamma}f_\beta - \frac{1}{\sin\beta}f_\gamma\right)\right](n\cdot u_{,a}) + \frac{1}{2}(e_{\alpha,a}\cdot f_\alpha)\left[n\cdot\left(\frac{1}{\sin\gamma}u_{,b} - \frac{1}{\sin\beta}u_{,c}\right)\right] \tag{77}$$

Corresponding expressions for χ_β and χ_γ are easily established. For lack of space we have to omit the proof, that rigid-body motions indeed give neither membrane nor bending strains.

4. INTERPOLATION OF THE MIDDLE SURFACE

a. Definition of Geometry at the Vertices

It can be assumed that the lines of principal curvature at the nodal points are known and that their directions are given by the unit vectors

$$e_A = \frac{\partial x}{\partial A}, \quad e_B = \frac{\partial x}{\partial B} \tag{78}$$

where the derivatives are taken with respect to the arc lengths on the principal curves. In the case of cylindrical shells or shells of revolution it is no problem to find the $e_A - e_B$ system. For a general surface we may apply the same mapping procedure as for the LUMINA element (Reference 3). To this purpose we only require the cartesian coordinates of a set of nodal or dummy points to establish a representation of the shell's middle surface by the Lagrangian interpolation polynomials $\pi(\xi^1, \xi^2)$. Following the solution of a simple (2 x 2) eigenvalue problem it is easy to transform the derivatives of $x(\xi^1, \xi^2)$ with respect to ξ^1 and ξ^2 to the so-called principal set

$$x \quad x_{,A} \quad x_{,B} \quad x_{,AA} \quad x_{,AB} \quad x_{,BB} \tag{79}$$

For the transformation of the second order derivatives we have to apply a technique corresponding to that of Equations 92 and 95 for specific details see Reference 19.

b. Definition of Geometry within an Element

To obtain the necessary data defining the geometry within an element we have to transform the nodal data 79 into the natural directions of the triangular shell element. Following Figure 29 we first introduce the unit vectors of the basic triangle i, j, k

$$j_\lambda = \frac{x_j - x_i}{\ell_\lambda} \quad ; \quad j_\mu = \frac{x_k - x_j}{\ell_\mu} \quad ; \quad j_\nu = \frac{x_i - x_k}{\ell_\nu} \tag{80}$$

We next determine at a typical vertex i the natural unit vectors $e_{\lambda i}$ and $e_{\nu i}$, using the conditions that $e_{\lambda i}$ ($e_{\nu i}$) lie in the plane $n_i - j_\lambda (n_i - j_\nu)$ and also in the tangential plane. We easily find

$$e_\lambda = \frac{j_\lambda - (n \cdot j_\lambda)\, n}{\left[1 - (n \cdot j_\lambda)^2\right]^{1/2}} \quad ; \quad e_\nu = \frac{j_\nu - (n \cdot j_\nu)\, n}{\left[1 - (n \cdot j_\nu)^2\right]^{1/2}} \tag{81}$$

where the subscript i is omitted. The actual interpolation procedure is carried out in Equation 98 using the TUBA 6 functions. To be consistent with the TUBA theory it is necessary to fix the measures at the vertices i, j, k using equations of the type

$$\frac{dx}{dt_\lambda} = \frac{1}{\ell_\lambda} \frac{\partial x}{\partial \zeta_\lambda} = \frac{1}{\ell_\lambda} x_{,\lambda} = \frac{1}{(e_\lambda \cdot j_\lambda)} e_\lambda \tag{82}$$

where t_λ is a distance measured parallel to j_λ in the basic triangle; see Figure 29. On the other hand dx/dt_λ has to be identical with e_λ. Therefore we have to set

$$x_{,\lambda} = \frac{\ell_\lambda}{(e_\lambda \cdot j_\lambda)} e_\lambda \quad \text{and correspondingly} \quad x_{,\nu} = \frac{\ell_\nu}{(e_\nu \cdot j_\nu)} e_\nu \tag{83}$$

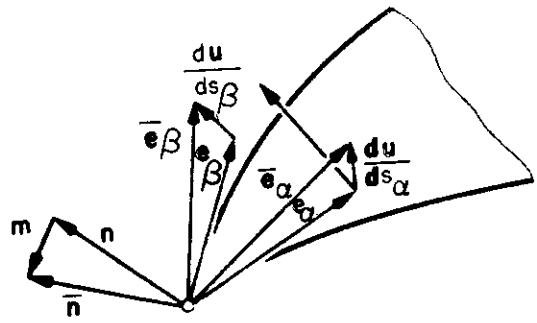

Figure 27. Change of Normal Vector due to Deformation

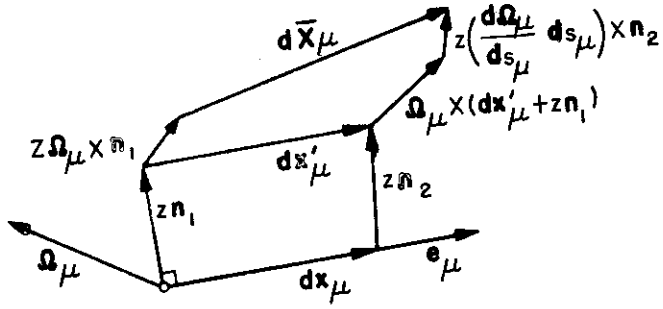

Figure 28. Total Natural Bending Strain

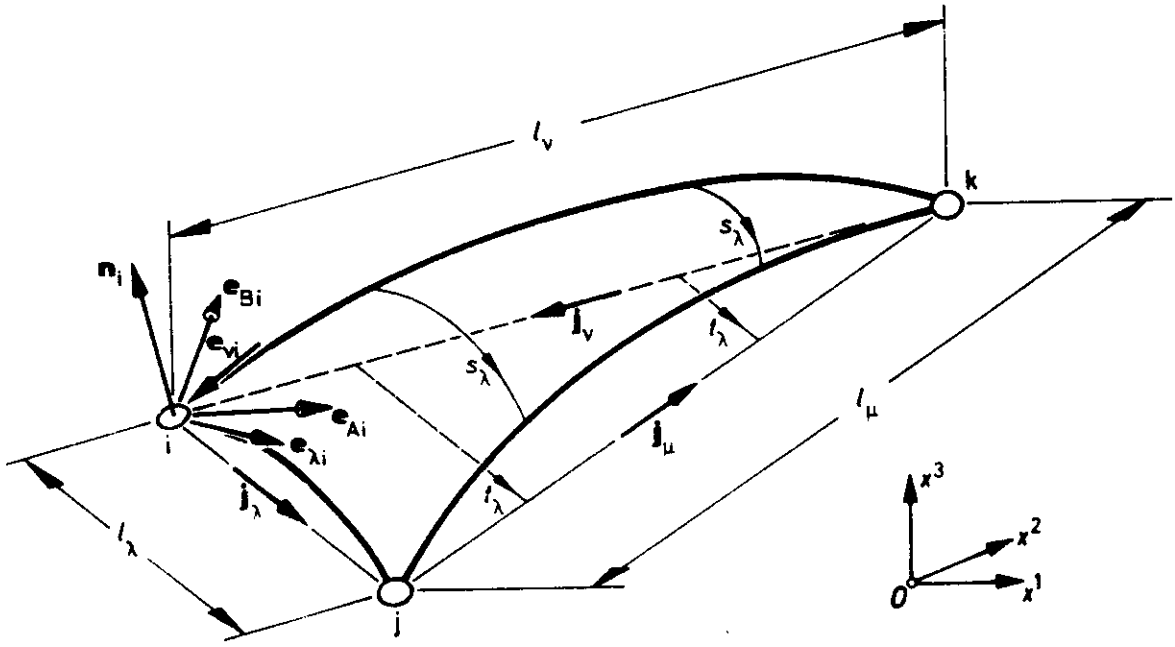

Figure 29. Natural Set of Geometric Data at Vertices

which yields for the associated measures at the vertex i

$$m_\lambda = \ell_\lambda \, (e_\lambda \cdot j_\lambda) \; ; \quad m_\nu = \ell_\nu / (e_\nu \cdot j_\nu) \tag{84}$$

To obtain the last m_μ at the vertex i we apply Equation 26 to find

$$e_\mu = -\frac{1}{m_\mu} (m_\lambda e_\lambda + m_\nu e_\nu) \tag{85}$$

and since $| e_\mu | = 1$

$$m_\mu = (m_\lambda^2 + 2 m_\lambda m_\nu (e_\lambda \cdot e_\nu) + m_\nu^2)^{1/2} \tag{86}$$

Using the unit vectors e_A and e_B of Equations 78 we find the evident identity

$$e_\lambda = (e_\lambda \cdot e_A) x_{,A} + (e_\lambda \cdot e_B) x_{,B} \tag{87}$$

and a corresponding one for e_λ. Equation 83 yield now the transformation of first order derivatives

$$\begin{aligned} x_u &= m_\lambda (e_\lambda \cdot e_A) x_{,A} + m_\lambda (e_\lambda \cdot e_B) x_{,B} \\ x_{,\nu} &= m_\nu (e_\nu \cdot e_A) x_{,A} + m_\nu (e_\nu \cdot e_B) x_{,B} \end{aligned} \tag{88}$$

which is used to define the operator transformation

$$\left\{ \frac{\partial}{\partial \zeta_\lambda} \quad \frac{\partial}{\partial \zeta_\nu} \right\} = F_i \quad \left\{ \frac{\partial}{\partial A} \quad \frac{\partial}{\partial B} \right\} \tag{89}$$

where

$$F_i = \begin{bmatrix} m_\lambda & m_\nu \end{bmatrix} \begin{bmatrix} e_\lambda \cdot e_A & e_\lambda \cdot e_B \\ e_\nu \cdot e_A & e_\nu \cdot e_B \end{bmatrix} \tag{90}$$

To extend the Transformation 90, which is exact, to second order derivatives we assume it to represent a transformation from an oblique system $\zeta_\mu - \zeta_\nu$ to an orthogonal one A - B in the tangential plane, ignoring any change of the unit vectors e_A and e_B. This leads to

$$\left\{ \frac{\partial^2}{\partial \zeta_\lambda^2} \quad \frac{\partial^2}{\partial \zeta_\lambda \partial \zeta_\nu} \quad \frac{\partial^2}{\partial \zeta_\nu^2} \right\} = \bar{S}_i \left\{ \frac{\partial^2}{\partial A^2} \quad \frac{\partial^2}{\partial A \partial B} \quad \frac{\partial^2}{\partial B^2} \right\} \tag{91}$$

where

$$\bar{S}_i = \begin{bmatrix} m_\lambda^2 & m_\lambda m_\nu & m_\nu^2 \end{bmatrix} \begin{bmatrix} (e_\lambda \cdot e_A)^2 & 2(e_\lambda \cdot e_A)(e \cdot e_B) & (e_\lambda \cdot e_B)^2 \\ (e_\lambda \cdot e_A)(e_\nu \cdot e_A) & (e_\lambda \cdot e_A)(e_\nu \cdot e_B) + (e_\lambda \cdot e_B)(e_\nu \cdot e_A) & (e_\lambda \cdot e_B)(e_\nu \cdot e_B) \\ (e_\nu \cdot e_A)^2 & 2(e_\nu \cdot e_A)(e_\nu \cdot e_B) & (e_\nu \cdot e_B)^2 \end{bmatrix} \tag{92}$$

However, it follows from Equation 23 that

$$\frac{\partial^2}{\partial \zeta_\mu^2} = \frac{\partial^2}{\partial \zeta_\lambda^2} + 2\,\frac{\partial^2}{\partial \zeta_\lambda\,\partial \zeta_\nu} + \frac{\partial^2}{\partial \zeta_\nu^2} \tag{93}$$

Thus, one may replace Transformation 91 by

$$\left\{ \frac{\partial^2}{\partial \zeta_\lambda^2} \quad \frac{\partial^2}{\partial \zeta_\mu^2} \quad \frac{\partial^2}{\partial \zeta_\nu^2} \right\} = \mathbf{S}_i \quad \left\{ \frac{\partial^2}{\partial A^2} \quad \frac{\partial^2}{\partial A\,\partial B} \quad \frac{\partial^2}{\partial B^2} \right\} \tag{94}$$

where

$$\mathbf{S}_i = \left[m_\lambda^2 \quad m_\mu^2 \quad m_\nu^2 \right] \begin{bmatrix} (e_\lambda \cdot e_A)^2 & 2(e_\lambda \cdot e_A)(e_\lambda \cdot e_B) & (e_\lambda \cdot e_B)^2 \\ (e_\mu \cdot e_A)^2 & 2(e_\mu \cdot e_A)(e_\mu \cdot e_B) & (e_\mu \cdot e_B)^2 \\ (e_\nu \cdot e_A)^2 & 2(e_\nu \cdot e_A)(e_\nu \cdot e_B) & (e_\nu \cdot e_B)^2 \end{bmatrix} \tag{95}$$

In establishing $\mathbf{S}_i$ Relations 85 and 86 have been used. Applying the Transformations 89 and 95 we can derive at each vertex from the principal set 79 the natural set

$$x \quad x_{,\lambda} \quad x_{,\nu} \quad x_{,\lambda\lambda} \quad x_{,\mu\mu} \quad x_{,\nu\nu} \tag{96}$$

c. Interpolation of the Middle Surface

In order to use the TUBA 6 interpolation scheme we require the (21 x 3) natural geometry matrix

$$\begin{aligned} \bar{x}_{IN} = \Big\{ & \bar{x}_1 \quad \bar{x}_2 \quad \bar{x}_3 \quad \bar{x}_{1,\alpha} \quad \bar{x}_{1,\gamma} \quad \bar{x}_{2,\beta} \quad \bar{x}_{2,\alpha} \quad \bar{x}_{3,\gamma} \quad \bar{x}_{3,\beta} \quad \bar{x}_{1,\alpha\alpha} \quad \bar{x}_{1,\gamma\gamma} \quad \bar{x}_{2,\beta\beta} \quad \bar{x}_{2,\alpha\alpha} \\ & \bar{x}_{3,\gamma\gamma} \quad \bar{x}_{3,\beta\beta} \quad \bar{x}_{1,\beta\beta} \quad \bar{x}_{2,\gamma\gamma} \quad \bar{x}_{3,\alpha\alpha} \quad \bar{x}_{4,\nu 3} \quad \bar{x}_{5,\nu 1} \quad \bar{x}_{6,\nu 2} \Big\} \\ = \Big\{ & x_{IN}^1 \quad x_{IN}^2 \quad x_{IN}^3 \Big\} \end{aligned} \tag{97}$$

The elements in Equation 98 are obtained by transposition of the column matrices 97 with the exception of $x_{4,\nu 3}$, $x_{5,\nu 1}$ and $x_{6,\nu 2}$ which are derived by the interpolation procedure of Equation 39 in Reference 12. Note that the eccentricity parameters $\mu_\alpha, \mu_\beta, \mu_\gamma$ refer to the basic points 4, 5, 6. The alternative formulation of x_{IN} in Equation 97 represents it as a matrix of three columns corresponding to each of the three cartesian coordinates. In accordance with Equations 6 and 24 of Reference 12, we find the current position vector x from the transformation

$$x^\dagger = \bar{x} = \omega\, A\, \bar{x}_{IN} \tag{98}$$

The (1 x 21) matrix ω which depends on ζ_1, ζ_2, ζ_3 and the (21 x 21) matrix A are given in Equation 31 and Figure 5 of Reference 12. The transformation 98 may be interpreted as defining three distinct surfaces $x^\rho(\zeta_1, \zeta_2, \zeta_3)$ over the basic triangle. The geometrical

data associated with adjoining triangular shell elements meeting at a nodal point are, however, deduced from a common smooth surface. It may hence be argued that the functions x^{ρ} and their first derivatives are continuous along the edges as in the case of the deflexions w of TUBA 6. It is of no consequence that the basic triangles are not in a plane but form a polyhedron surface. Consequently we have interpolated the actual middle surface of the shell in such a manner that no folds are generated. The second derivatives are of course, in general, discontinuous across the edges with the exception of the vertices. We may also define a (63 x 1) matrix

$$x_{IN} = \left\{ x_1 \quad x_2 \quad x_3 \quad x_{1,\alpha} \quad x_{1,\gamma} \text{ ------ } x_{3,\alpha\alpha} \quad x_{4,\nu 3} \quad x_{5,\nu 1} \quad x_{6,\nu 2} \right\} \tag{99}$$

which yields

$$x = \overline{3} \left[\omega \quad A \right] x_{IN} = D x_{IN} \tag{100}$$

where the operator 3 is defined in Reference 5.

5. INTERPOLATION OF DISPLACEMENTS

a. Displacement Matrix at the Nodal points

At a typical vertex i of a triangular shell element i, j, k we introduce the (6 x 3) displacement matrix

$$\bar{\rho}_i = \left\{ \bar{u} \quad \bar{u}_{,A} \quad \bar{u}_{,B} \quad \bar{u}_{,AA} \quad \bar{u}_{,AB} \quad \bar{u}_{,BB} \right\}_i \tag{101}$$

Applying the Transformations 89 and 94 we deduce the natural displacement matrix at the vertex i

$$\bar{\rho}_{Ni} = \left[1 \quad F_i \quad S_i \right] \bar{\rho}_i \tag{102}$$

with

$$\bar{\rho}_{Ni} = \left\{ \bar{u} \quad \bar{u}_{,\lambda} \quad \bar{u}_{,\nu} \quad \bar{u}_{,\lambda\lambda} \quad \bar{u}_{,\mu\mu} \quad \bar{u}_{,\nu\nu} \right\}_i \tag{103}$$

At the intermediate nodal points, p, q, r (see Figure 29) we have to define a (1 x 3) displacement matrix in accordance with the TUBA procedure. For instance, at the point

$$\bar{\rho}_p = \bar{u}_{p,nk} \tag{104}$$

The differentiation with respect to ν_k is fixed by operators of the type

$$\frac{\partial}{\partial \nu_3} = 2\frac{\partial}{\partial \zeta_3} - \left(\frac{\partial}{\partial \zeta_1} + \frac{\partial}{\partial \zeta_2}\right) - \mu_\alpha\left(\frac{\partial}{\partial \zeta_1} + \frac{\partial}{\partial \zeta_2}\right) \tag{105}$$

see also Equations 16 and 17 of Reference 12. No further transformations will be applied to these freedoms.

b. The Complete Displacement Matrix of the Element

We next introduce the complete (21 x 3) ρ_I matrix for a shell element in the form

$$\bar{\rho}_I = \left\{\bar{\rho}_1 \quad \bar{\rho}_2 \quad \bar{\rho}_3 \quad \bar{\rho}_4 \quad \bar{\rho}_5 \quad \bar{\rho}_6\right\} \tag{106}$$

where ρ_1, ρ_2, ρ_3 are given in Equations 102 and ρ_4, ρ_5, ρ_6 in Equation 105. The complete natural displacement matrix is given by

$$\bar{\rho}_{NI} = \left\{\bar{\rho}_{N1} \quad \bar{\rho}_{N2} \quad \bar{\rho}_{N3} \quad \frac{4\Omega}{\ell_\alpha}\bar{\rho}_4 \quad \frac{4\Omega}{\ell_\beta}\bar{\rho}_5 \quad \frac{4\Omega}{\ell_\gamma}\bar{\rho}_6\right\} \tag{107}$$

Extending the Transformation 103 we find

$$\bar{\rho}_{NI} = \bar{X}_S \; \bar{\rho}_I \tag{108}$$

with

$$\bar{X}_S = B_6 \; \bar{X}_B \tag{109}$$

where B_6 is given in Equation 31 of Reference 12 and

$$\bar{X}_B = \begin{bmatrix} 1 & \cdot & \cdot & \cdot & \cdot & \cdot & \cdot & \cdot & \cdot & \cdot \\ \cdot & \cdot & \cdot & 1 & \cdot & \cdot & \cdot & \cdot & \cdot & \cdot \\ \cdot & \cdot & \cdot & \cdot & \cdot & \cdot & 1 & \cdot & \cdot & \cdot \\ \cdot & F_1 & \cdot & \cdot & \cdot & \cdot & \cdot & \cdot & \cdot & \cdot \\ \cdot & \cdot & \cdot & \cdot & F_2 & \cdot & \cdot & \cdot & \cdot & \cdot \\ \cdot & \cdot & \cdot & \cdot & \cdot & \cdot & \cdot & F_3 & \cdot & \cdot \\ \cdot & \cdot & S_1 & \cdot & \cdot & \cdot & \cdot & \cdot & \cdot & \cdot \\ \cdot & \cdot & \cdot & \cdot & \cdot & S_2 & \cdot & \cdot & \cdot & \cdot \\ \cdot & \cdot & \cdot & \cdot & \cdot & \cdot & \cdot & \cdot & S_3 & \cdot \\ \cdot & \cdot & \cdot & \cdot & \cdot & \cdot & \cdot & \cdot & \cdot & 4\Omega\ell^{-1} \end{bmatrix} \quad (21 \times 21) \tag{110}$$

Also

$$\ell = \left[\ell_\alpha \quad \ell_\beta \quad \ell_\gamma\right] \tag{111}$$

Alternatively we can define the two (18 x 1) matrices of displacements at a nodal point

$$\rho_i = \left\{ u \quad u_{,A} \quad u_{,B} \quad u_{,AA} \quad u_{,AB} \quad u_{,BB} \right\}_i \tag{112}$$

$$\rho_{Ni} = \left\{ u \quad u_{,\lambda} \quad u_{,\nu} \quad u_{,\lambda\lambda} \quad u_{,\mu\mu} \quad u_{,\nu\nu} \right\}_i \tag{113}$$

and the (3 x 1) matrix at nodal point

$$\rho_p = u_{p,nk} \tag{114}$$

These form the alternative (63 x 1) complete displacement matrices

$$\rho_I = \left\{ \rho_1 \quad \rho_2 \quad \rho_3 \quad \rho_4 \quad \rho_5 \quad \rho_6 \right\} \tag{115}$$

and

$$\rho_{NI} = \left\{ \rho_{N1} \quad \rho_{N2} \quad \rho_{N3} \quad \frac{4\Omega}{\ell_\alpha}\rho_4 \quad \frac{4\Omega}{\ell_\beta}\rho_5 \quad \frac{4\Omega}{\ell_\gamma}\rho_6 \right\} \tag{116}$$

The Transformation 109 becomes then

$$\rho_{NI} = 3\Big] \; \bar{X}_S \, \rho_I = X_S \rho_I \tag{117}$$

The conditioning of the stiffness matrix may be improved considerably by introducing the displacement matrix

$$\rho_I = \left[C_{1e} \quad C_{2e} \quad C_{3e} \quad I_9 \right] \rho = C_e \rho \tag{118}$$

where a typical

$$C_{ie} = \left[C_i \quad C_i \quad C_i \quad C_i \quad C_i \quad C_i \right] \tag{119}$$

and

$$C_i = \left[e_A \quad e_B \quad n \right]_i \tag{120}$$

This transformation relates the global cartesian displacement $u = \{u^1 u^2 u^3\}$ to the local system $n - e_A - e_B$ of principal curvatures. For brevity we restrict ourselves in the above derivation to shallow shells. The extension to more general surfaces is straightforward, see Reference 19.

c. Interpolation Scheme of Displacements

As in the case of the interpolation of the middle surface the current displacement vector u is defined by the transformations

$$\bar{u} = \omega A \bar{\rho}_{NI} \qquad \text{or} \qquad u = D \rho_{NI} \tag{121}$$

where $\mathbf{D}$ is given in Equation 101. Note that the (21 x 3) matrices $\bar{\rho}_{NI}$ of a pure translation $\mathbf{U}_0$ or a rigid rotation through a vector $\boldsymbol{\phi}$ with

$$\mathbf{u}_0 = \left\{ u_0^1 \quad u_0^2 \quad u_0^3 \right\} \; ; \qquad \boldsymbol{\phi} = \left\{ \phi^1 \quad \phi^2 \quad \phi^3 \right\} \tag{122}$$

have to be defined as

$$\bar{\rho}_{NIo} = \left\{ u_0^1 \quad u_0^1 \quad u_0^1 \quad 0_{18,3} \right\} \tag{123}$$

or

$$\bar{\rho}_{NI\phi} = \left[\phi^2 x_{NI}^3 \quad -\phi^3 x_{NI}^2 \quad \phi^3 x_{NI}^1 \quad -\phi^1 x_{NI}^3 \quad \phi^1 x_{NI}^2 \quad -\phi^2 x_{NI}^1 \right] \tag{124}$$

respectively, where $\mathbf{x}_{NI}$ are the (21 x 1) matrices which form the columns of $\bar{\mathbf{x}}_{NI}$ in Equation 98. Using the Definitions (123) and (124) the TUBA 6 interpolation scheme guarantees that at any point within the element the relations $\mathbf{U} = \mathbf{U}_0$, $\mathbf{U} = \boldsymbol{\phi} \times \mathbf{x}$ hold and that there are zero strains.

6. STIFFNESS MATRIX

a. Virtual Work

If an element of volume $dz \; d\Omega$ is subjected to a strain ϵ_μ the virtual work due to a stress $E K_{\mu\nu} \epsilon_\nu$ is

$$d^3 W = E K_{\mu\nu} \epsilon_\mu \epsilon_\nu \; dz \; d\Omega \tag{125}$$

where E is standing for Young's modulus and $K_{\mu\nu}$ is one of the natural material stiffness coefficients which form the matrix $\mathbf{K}_N$ (Reference 1). To evaluate Equation 125 we can apply the formulae of the standard shell theory (References 31 and 32) to the direct component strains. We obtain after integration over the thickness t

$$d^2 W = E K_{\mu\nu} \left(t \, \epsilon_{\mu o} \, \epsilon_{\nu o} + \frac{t^3}{12} \chi_\mu \chi_\nu \right) d\Omega \tag{126}$$

The variation of the elements of arc length and area with z can be neglected in the case of thin shells with $t/R \ll 1$, R being a typical measure of the radii of curvature. It is worth mentioning that the natural stiffness concept leads also to a variation of $\mathbf{K}_N$ with z, due to a change of the enclosed angle between $\mathbf{e}_\mu'$ and $\mathbf{e}_\nu'$, but this influence is once more of the order of magnitude t/R (Reference 19).

b. Membrane Stiffness

Using the interpolation scheme of Equation 121 we are able to represent the Relation 52 for the natural membrane strain matrix ϵ_{NO} as the linear transformation

$$\epsilon_{No} = m^{-2} \; a_M \; \rho_{NI} \tag{127}$$

Here

$$m = \left[m_\alpha \quad m_\beta \quad m_\gamma \right] \tag{128}$$

and

$$a_M = m \left\{ e^t_\alpha \; D_{,\alpha} \quad e^t_\beta \; D_{,\beta} \quad e^t_\gamma \; D_{,\gamma} \right\} \quad (3 \times 63) \tag{129}$$

where

$$D_{,\mu} = \overline{3} \left[\omega_{,\mu} \; A \right] \tag{130}$$

The membrane stiffness corresponding to the displacement matrix ρ_{NI} is now

$$k_M = E \int_\Omega t \; a^t_M \; \lambda_N \; a_M \, d\Omega \qquad (63 \times 63) \tag{131}$$

Here

$$\lambda_N = m^{-2} \; K_N \; m^{-2} \qquad (3 \times 3) \tag{132}$$

Naturally, the Integral 131 and all following corresponding expressions have to be evaluated numerically.

c. Bending Stiffness

Introducing the Interpolation Scheme 121 into Equation 77 we find the linear transformation

$$\chi_N = m^{-2} \; a_B \; \rho_{NI} \tag{133}$$

where

$$a_B = \left\{ a_{B\alpha} \quad a_{B\beta} \quad a_{B\gamma} \right\} \qquad (3 \times 63) \tag{134}$$

Restricting our considerations to the typical matrix $a_{B\alpha}$ and omitting the subscript $B\alpha$ on the righthand side, we may write

$$a_{B\alpha} = a_{\alpha\alpha} + a_{\alpha} + a_{\beta} + a_{\gamma} \qquad (1 \times 63) \tag{135}$$

We easily establish

$$\begin{aligned} a_{\alpha\alpha} &= -n^{t} \; D_{,\alpha\alpha} \quad ; & a_{\alpha} &= \frac{1}{m_{\alpha}} \; b_{\alpha}^{t} \; D_{,\alpha} \\ a_{\beta} &= \frac{1}{m_{\beta}} \; b_{\beta}^{t} \; D_{,\beta} \quad ; & a_{\gamma} &= \frac{1}{m_{\gamma}} \; b_{\gamma}^{t} \; D_{,\gamma} \end{aligned} \tag{136}$$

where

$$\begin{aligned} b_{\alpha} &= (x_{,\alpha\alpha} \cdot n)\, e_{\alpha} - \frac{1}{2}\left[x_{,\alpha\alpha} \cdot \left(\frac{1}{\sin\gamma} f_{\beta} - \frac{1}{\sin\beta} f_{\gamma}\right)\right] n \\ b_{\beta} &= \frac{1}{2\sin\gamma}\,(x_{,\alpha\alpha} \cdot f_{\alpha})\, n \;, \qquad b_{\gamma} = -\frac{1}{2\sin\beta}\,(x_{,\alpha\alpha} \cdot f_{\alpha})\, n \end{aligned} \tag{137}$$

Also

$$x_{,\alpha\alpha} = D_{,\alpha\alpha} \; x_{NI} \tag{138}$$

The bending stiffness corresponding to the displacement matrix ρ_{NI} is therefore

$$k_{B} = \frac{E}{12} \int_{\Omega} t^{3} \; a_{B}^{t} \; \lambda_{N} \; a_{B} \; d\Omega \qquad (63 \times 63) \tag{139}$$

d. Complete Stiffness Matrix

The complete stiffness matrix based on the displacement matrix ρ (Equation 119) is finally

$$k = C_{e}^{t} \; X_{S}^{t} \left[k_{M} + k_{B}\right] X_{S} \; C_{e} \qquad (63 \times 63) \tag{140}$$

SECTION IV

ELASTOPLASTIC ANALYSIS

1. GENERAL CONSIDERATIONS

The matrix displacement method covers not only linear, elastic (Hookean) behaviour, but also in conjunction with step-wise procedures, nonlinear conditions which occur, for example, in nonelastic and large displacement or strain problems. This chapter presents an extension of the theory, first given in Reference 36, for handling nonlinear stress-strain relationships due to plastic deformations and work hardening. In order to limit the scope of this paper, we do not consider the effects of large displacements and strains, which often occur in such problems, although for these purposes the concept of geometrical stiffness has been developed (References 1, 6 and Section V).

In order to describe clearly the principles of our method, we restrict ourselves to the von Mises yield criterion for isotropic materials and the Prandtl-Reuss equations, which together lead to a mathematically and physically consistent theory of yield phenomena. The incremental stress-strain relations corresponding to stepwise small changes in the loading are written in a matrix formulation suitable for computer use.

As pointed out in previous publications (Reference 36) it is advantageous to apply the so-called method of initial loads (Reference 1) for the representation of plastic strains. This technique allows the use of a constant stiffness matrix for constant temperature and small displacements. The calculation of initial strains and the elastic analysis with initial strains are described in a general manner, which can be applied to any element.

The determination of the plastic initial strains is somewhat complicated because the increment of plastic strain is dependent on the stress increment, which again depends on the current value of plastic strain. These difficulties can, however, be circumvented by the method of this report. The application of the procedure is illustrated on the analysis of a cracked plate.

2. INCREMENTAL STRESS-STRAIN RELATIONSHIPS

a. Stress and Strain Vectors

We consider only a three-dimensional continuum, where strains and stresses are described using the (6 x 1) column matrices of cartesian components

$$\epsilon = \left\{ \epsilon_{xx} \;\; \epsilon_{yy} \;\; \epsilon_{zz} \;\; \frac{1}{\sqrt{2}} \epsilon_{xy} \;\; \frac{1}{\sqrt{2}} \epsilon_{yz} \;\; \frac{1}{\sqrt{2}} \epsilon_{zx} \right\} \tag{142}$$

$$\sigma = \left\{ \sigma_{xx} \;\; \sigma_{yy} \;\; \sigma_{zz} \;\; \sqrt{2}\sigma_{xy} \;\; \sqrt{2}\sigma_{yz} \;\; \sqrt{2}\sigma_{zx} \right\} \tag{143}$$

These definitions guarantee the duality of static and kinematic transformations, as shown in Reference 1. Lack of space precludes giving the most elegant natural formulation, but we suggest for this purpose a perusal of Reference 23. The nonelastic strains, which are to be understood here exclusively as plastic strains, and the total strains are denoted by the vectors η and γ respectively. Thus we have

$$\gamma = \epsilon + \eta \tag{144}$$

Clearly η and γ must be written analogously to ϵ of Equation 142. For linearly elastic material

$$\sigma = \mathbf{E}\,\epsilon \tag{145}$$

where $\mathbf{E}$ is the (6 x 6) material stiffness matrix (Reference 1), which in the isotropic case is

$$\mathbf{E} = 2G\left[\mathbf{I}_6 + \frac{\nu}{1-2\nu} \mathbf{E}_{3,3} \right] \tag{146}$$

with the (6 x 6) unit matrix $\mathbf{I}_6$ and $\mathbf{E}_{3,3} = \mathbf{e}_{3,3}\mathbf{e}_{3,3}^{\dagger}$, where $\mathbf{e}_{3,3}$ is the (6 x 1) column matrix $\mathbf{e}_{3,3} = \{111000\}$. G and ν denote the shear modulus and Poisson's ratio respectively.

The vectors σ and γ can be divided into so-called hydrostatic and deviatoric parts

$$\sigma = \sigma_H + \sigma_D \;\; ; \;\; \gamma = \gamma_H + \gamma_D \tag{147}$$

where

$$\sigma_H = \frac{1}{3}(\sigma_{xx} + \sigma_{yy} + \sigma_{zz})\,\mathbf{e}_{3,3} \;\; ; \;\; \gamma_H = \frac{1}{3}(\gamma_{xx} + \gamma_{yy} + \gamma_{zz})\,\mathbf{e}_{3,3} \tag{148}$$

are the hydrostatic stress and the delation respectively. To fulfill Equation 147 we set for the deviatoric vectors

$$\sigma_D = \mu_D \sigma \;\; ; \;\; \gamma_D = \mu_D \gamma \tag{149}$$

where

$$\mu_D = I_6 - \frac{1}{3} E_{3,3} \tag{150}$$

For any ν it is easy to prove that

$$E \mu_D = 2G \mu_D \tag{151}$$

Note also the useful relation

$$\mu_D \mu_D = \mu_D \tag{152}$$

for the symmetric (6 x 6) matrix μ_D

b. Yield Criterion and Plastic Strain Increments

Using the Definition 150 of the deviatoric stresses σ_D and Equation 152 the von Mises criterion, which is valid for isotropic materials, takes the simple form

$$\bar{\sigma}^2 = \frac{3}{2} \sigma_D^t \sigma_D = \frac{3}{2} \sigma^t \mu_D \sigma \tag{153}$$

where $\bar{\sigma}$ is the so-called equivalent stress. Condition 153 for the stresses σ says that plastic deformations occur when $\bar{\sigma}$ reaches a critical value, which is initially equal to the elastic limit σ_ℓ. Subsequent yielding takes place if $\bar{\sigma}$ becomes greater than the maximum value $\bar{\sigma}_{max}$ previously reached in the point considered. Corresponding to $\bar{\sigma}$ we now introduce the equivalent strain

$$\bar{\gamma}^2 = \frac{2}{3} \gamma_D^t \gamma_D = \frac{2}{3} \gamma^t \mu_D \gamma \tag{154}$$

For a uniaxial stress state one finds

$$\bar{\sigma} = \sigma \; ; \; \bar{\gamma} = \gamma \quad ; \quad \bar{\eta} = \eta = \gamma - \sigma / E \qquad (E = \text{Young's modulus}) \tag{155}$$

One sees therefore that the assumption of plastic isotropy allows the extraction of all information about the yield condition in a three-dimensional stress state from a simple uniaxial tension test.

The increments of plastic strain η_D of a typical loading step are calculated using the Pandtl-Reuss equations

$$\eta_\Delta = \beta_\Delta \sigma_D = \beta_\Delta \mu_D \sigma \tag{156}$$

This establishes a consistent theory in connexion with the von Mises Criterion 153. Applying Equations 153 and 154 to compare the three-dimensional with the uniaxial stress state we find for the so-called plasticity factor β_Δ.

$$\beta_\Delta = \frac{3}{2} \frac{1}{\zeta} \frac{\bar{\sigma}_\Delta}{\bar{\sigma}} \tag{157}$$

where ζ is the slope of the $\sigma-\eta$ diagram of a uniaxial test, as shown in Figure 30. All unloadings, of course, must be calculated elastically. This is done automatically by setting $\frac{1}{\zeta} = 0$, if $\sigma \leq \sigma_{max}$ or σ_i. The equivalent stress increments can be found either directly from $\bar{\sigma}_\Delta = \bar{\sigma} - \bar{\sigma}_{max}$ or by differentiating Equation 153. This leads to

$$\bar{\sigma}_\Delta = \frac{3}{2} \frac{1}{\bar{\sigma}} \sigma^t \mu_D \sigma_\Delta \tag{158}$$

where σ_Δ is the incremental stress vector. Expression 158 is especially suitable for the following theory because it enforces a complete linearization of the incremental elastoplastic stress-strain relations.

c. Initial Loads

It is advantageous to represent the effect of the plastic strains by a corresponding set of initial loads. These simulate, in effect, an elastic suppression of the initial strains within each element. The total strain can be obtained for any type of finite element from the vector ρ of element freedoms by a transformation

$$\gamma = a \rho \tag{159}$$

At the same time the initial strains of any point within an element may be determined from a characteristic set of initial strains η_c using an interpolation transformation

$$\eta = b \eta_c \tag{160}$$

where η_c is a super column matrix containing the vectors η of a certain number of suitable points. The virtual work principle yields now for the initial load vector J associated with ρ

$$J = -\int_V a^t E \eta \, dV = -h \eta_c \tag{161}$$

where

$$h = \int_V a^t E b \, dV \tag{162}$$

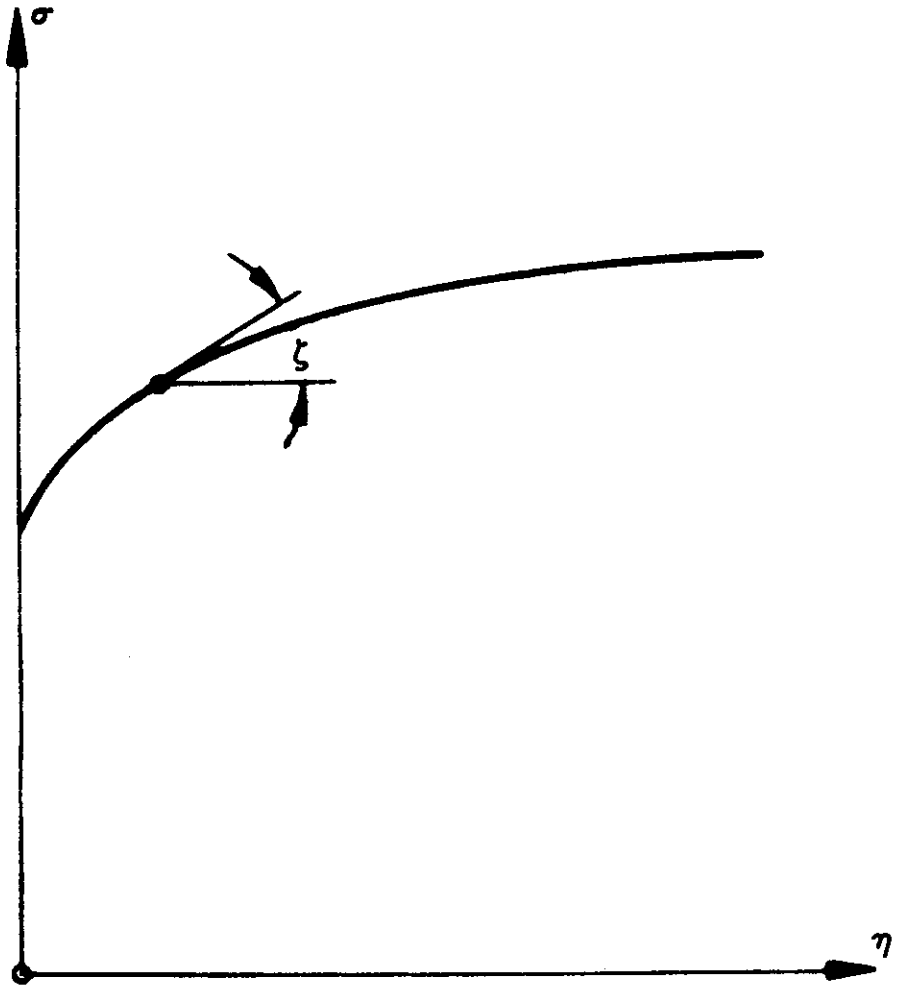

Figure 30. Typical $\sigma - \eta$ diagram (above)

In an analogous fashion, a set of total strains describing uniquely the deformation of an element may be set up in the form

$$\gamma_c = a_c \rho \tag{163}$$

where a_c is a column supermatrix built up from the matrices a of the selected characteristic points. For simplicity in what follows we omit the subscript c and do not introduce additional subscripts or new symbols when expanding matrices defined elementwise to complete structural matrices.

The condition of equilibrium for a structure subjected to external loads $\mathbf{R}$ and initial loads $\mathbf{J}$ -applied to the elements - is

$$\mathbf{R} = \mathbf{K}\,\mathbf{r} - \mathbf{a}^{\dagger}\,\mathbf{J} \tag{164}$$

where $\mathbf{r}$ is the displacement matrix corresponding to $\mathbf{R}$, $\mathbf{K}$ the elastic stiffness matrix, and $\mathbf{a}$ a Boolean matrix relating the degrees of freedom of the elements to those of the structure (Reference 1). We deduce from Equation 164.

$$\mathbf{r} = \mathbf{K}^{-1}(\mathbf{R} - \mathbf{a}^{\dagger}\,\mathbf{J} \tag{165}$$

The total displacement vector $\boldsymbol{\rho}_T$ of the elements is found from the Boolean Transformation

$$\boldsymbol{\rho}_T = \mathbf{a}\,\mathbf{r} \tag{166}$$

which yields for the total strains

$$\boldsymbol{\gamma} = \boldsymbol{\alpha}\,\boldsymbol{\rho}_T \tag{167}$$

Therefore the elastic strains are

$$\boldsymbol{\epsilon} = \boldsymbol{\alpha}\boldsymbol{\rho}_T - \boldsymbol{\eta} \tag{168}$$

and the stresses

$$\boldsymbol{\sigma} = \mathbf{E}(\boldsymbol{\alpha}\boldsymbol{\rho}_T - \boldsymbol{\eta}) \tag{169}$$

d. Incremental Stress-Strain Relationships for a Complete Structure

Condensing Equations 162, 166 to 169 for a structure subjected to external forces $\mathbf{R}_\Delta$ and plastic initial strains $\boldsymbol{\eta}_\Delta$, one obtains the stress increments

$$\boldsymbol{\sigma}_\Delta = \mathbf{E}\,\boldsymbol{\alpha}\,\mathbf{a}\,\mathbf{K}^{-1}\,\mathbf{R}_\Delta + \mathbf{E}(\boldsymbol{\alpha}\,\mathbf{a}\,\mathbf{K}^{-1}\,\mathbf{a}^{\dagger}\,\mathbf{h} - \mathbf{I})\,\boldsymbol{\eta}_\Delta \tag{170}$$

where $\mathbf{I}$ is a unit matrix. Using Equations 156 to 158 it follows that

$$\boldsymbol{\eta}_\Delta = \mathbf{H}\,\mathbf{R}_\Delta + \mathbf{G}\,\boldsymbol{\eta}_\Delta \tag{171}$$

where, in agreement with Equation 170

$$\mathbf{H} = 2G\,\boldsymbol{\zeta}^{-1}\,\mathbf{S}\,\mathbf{S}^{\dagger}\,\boldsymbol{\alpha}\,\mathbf{a}\,\mathbf{K}^{-1} \quad ; \quad \mathbf{G} = 2G\,\boldsymbol{\zeta}^{-1}\,\mathbf{S}\,\mathbf{S}^{\dagger}\,\mathbf{T} \tag{172}$$

with

$$\mathbf{S} = \frac{3}{2}\,\bar{\sigma}^{-1}\,\mu_D\,\boldsymbol{\sigma} \quad ; \quad \mathbf{T} = \boldsymbol{\alpha}\,\mathbf{a}\,\mathbf{K}^{-1}\,\mathbf{a}^{\dagger}\,\mathbf{h} - \mathbf{I} \tag{173}$$

The material stiffness $\mathbf{E}$ has been eliminated using Equation 151. All slopes ζ of the $\sigma-\eta$ diagram are collected in the diagonal matrix $\boldsymbol{\zeta}$. Note that by definition $\boldsymbol{\zeta}^{-1}$ has nonzero elements only at such points where further plastic deformation occurs. The matrix $\mathbf{S}$ is a diagonal supermatrix whose elements are the vectors

$$\mathbf{S} = \frac{3}{2}\,\frac{1}{\bar{\sigma}}\,\boldsymbol{\mu}_D\boldsymbol{\sigma} = \frac{3}{2}\,\frac{1}{\bar{\sigma}}\,\boldsymbol{\sigma}_D \tag{174}$$

The operation $\mathbf{SS}^t$ represents therefore a projection of the elastic strain vector $\boldsymbol{\epsilon}$ onto the normalized vector $\frac{1}{\bar{\sigma}}\boldsymbol{\sigma}_D$. We also observe that the transformation matrix $\mathbf{T}$ yields the elastic strains $\boldsymbol{\epsilon}$ due to any initial strains $\boldsymbol{\eta}$ via the relation

$$\boldsymbol{\epsilon} = \mathbf{T}\boldsymbol{\eta} \tag{175}$$

In Equation 171 $\mathbf{HR}_\Delta$ stands for the increments of plastic strain calculated from stress increments entirely elastic and arising from the load $\mathbf{R}_\Delta$. This contribution to $\boldsymbol{\eta}_\Delta$ can thus be easily calculated without first forming $\mathbf{H}$. The second part $\mathbf{G}\boldsymbol{\eta}_\Delta$ shows that plastic initial strain increments $\boldsymbol{\eta}_\Delta$ themselves produce further plastic deformation. Therefore it is necessary to know $\mathbf{G}$ explicitly in order to resolve the system of Equation 171 for $\boldsymbol{\eta}_\Delta$

3. ITERATIVE METHODS OF ELASTOPLASTIC ANALYSIS

a. The Basic Problem of Iterative Techniques

The methods of elastoplastic analysis described in Reference 36 use estimated starting values $\boldsymbol{\eta}_{\Delta-}$ for $\boldsymbol{\eta}_\Delta$ on the right hand side of Equation 171. This procedure enables us to compute improved plastic strain increments $\boldsymbol{\eta}_{\Delta+}$ without knowing $\mathbf{G}$ explicitly. To examine this point further we rewrite Equation 171 in the form

$$\boldsymbol{\eta}_{\Delta+} = \mathbf{HR}_\Delta + \mathbf{G}\boldsymbol{\eta}_{\Delta-} \tag{176}$$

There are two possible methods of evaluating Equation 176. These may be called the direct incremental method (DIM) and the normal iterative method (NIM). DIM uses the improved plastic strains $\boldsymbol{\eta}_{\Delta+}^{(i)}$ of a typical loading step i as starting values $\boldsymbol{\eta}_{\Delta-}^{(i+1)}$ of the following step. On the other hand NIM iterates within each loading step using as intial $\boldsymbol{\eta}_{\Delta-}$ the results of the preceding iteration until convergence is found. This can be understood as an iterative solution of Equation 171, which can converge only if all diagonal elements G_{ii} of $\mathbf{G}$ are less than 'one' as proved in standard matrix theory. However, this condition is not fulfilled in most practical problems. For ductile metals ζ decreases, in general, exponentially with increasing equivalent stress. Following the second of Equation 172 $1/\zeta$ is directly a multiplier of the diagonal elements of $\mathbf{G}$. Therefore, with increasing load, a point will be reached at which

any one of the G_{ii} may become greater than "one". Especially in three-dimensional problems it is even possible for T in Equation 173 to have such large diagonal elements that the iteration does not converge for any reasonable value of ζ. It is now obvious that the matrix G has to be considered in order to develop a successful method of solution for plastic problems.

b. Improved Iterative Method

In contrast to NIM we denote the procedure which uses G as an improved iterative method (VIM). The calculation of G from Relations 172 and 173 involves extensive numerical computations, especially for the complete inversion of K. The dimensions of G, however, can be readily reduced by a factor of six for the three-dimensional case by introducing the scalar plasticity factors β_Δ instead of the vectors η_Δ in Equation 171. This leads to

$$G_\beta = 2G\,\zeta^{-1}\,S^t\,T\,S \tag{177}$$

Obviously a numerical evaluation of Equation 176 is only economical if an overwhelming part of the structure is plastically deformed. In most real problems, however, yielding occurs in relatively small regions near notches or cracks. We require then only a certain part of G, obtained from

$$\bar{G} = c\,G\,c^t \tag{178}$$

where c is a Boolean (N x n) matrix which selects the N characteristic points where further yielding takes place, out of a total of, n characteristic points. Rewriting Equation 171 in the functional form

$$\eta_\Delta = \phi\,(\eta_\Delta) \tag{179}$$

it is easy to see that G is the gradient matrix of ϕ, i.e.

$$G = \frac{\partial \phi}{\partial \eta_\Delta} \tag{180}$$

Differentiation with respect to matrices is defined in Reference 1. Since it is not difficult to determine values of ϕ for any η_Δ, G can in practice be replaced approximately by difference quotients computed from modified vectors $\eta_{\Delta V}$. Let us assume that we know an approximate value $\eta_{\Delta 0}$ with N plasticity factors $\beta_\Delta \neq 0$. Then ϕ is calculated not only for $\eta_{\Delta 0}$ alone but also additionally for N modified vectors $\eta_{\Delta V}$ in each of which one β_Δ is slightly changed.

From the differences $\phi(\eta_{\Delta V}) - \phi(\eta_{\Delta 0})$ one may derive gradients, sufficiently accurate to ensure convergence of the iteration described below. This method consumes little more computer time as it simply requires considering N + 1 loading cases at one time to find of Equation 178.

Because the restricted $\bar{G}$ is now not exact, and even depends on the starting values $\eta_{\Delta 0}$, it is necessary to solve Equation 171 using once more an iterative technique. Noting that in n - N points β_Δ^j s vanish, and applying again the shorthand Notation 180, the so-called VIM procedure for a typical iteration step i to i + 1 can be written most concisely in the form

$$\eta_\Delta^{(i+1)} = \eta_\Delta^{(i)} - d\left[\eta_\Delta^{(i)} - \phi(\eta_\Delta^{(i)})\right] - c^t\left[I - G\right]^{-1} c\left[\eta_\Delta^{(i)} - \phi(\eta_\Delta^{(i)})\right] \qquad (181)$$

where **d** is a Boolean diagonal matrix eliminating those characteristic points at which **G** is applied. For further details see Reference 24.

c. Example of Cracked Plate

An interesting example for the application of VIM is a rectangular plate with a side ratio 2:1, which is cracked across the middle third of its width and which is loaded in the longer (axial) direction with a uniform tensile stress σ_0. Figure 31 shows a quarter of the plate and its idealization with TRIM 6 elements [1]. We have used the σ-η diagram of a 2024-T3 aluminium alloy, which can be closely represented by the modified Ramberg-Osgood relationship,

$$\eta = \frac{1.1\sigma_\ell}{mE}\left[\left(\frac{\sigma}{1.1\sigma_\ell}\right)^m - \left(\frac{1}{1.1}\right)^m\right] \qquad (182)$$

with $E = 11.4 \times 10^6$ lbf/in^2, $\sigma_\ell = 34{,}500$ lbf/in^2 and an exponent m = 10. Computer applications confirm that this problem can be solved for the exponential stress-strain Law 182 only if the VIM technique is applied. Figure 32 show, for various values of the tensile loading **G**, typical curves of constant normal stress σ_{yy} and equivalent stress $\bar{\sigma}$, and also the plastically deformed zone.

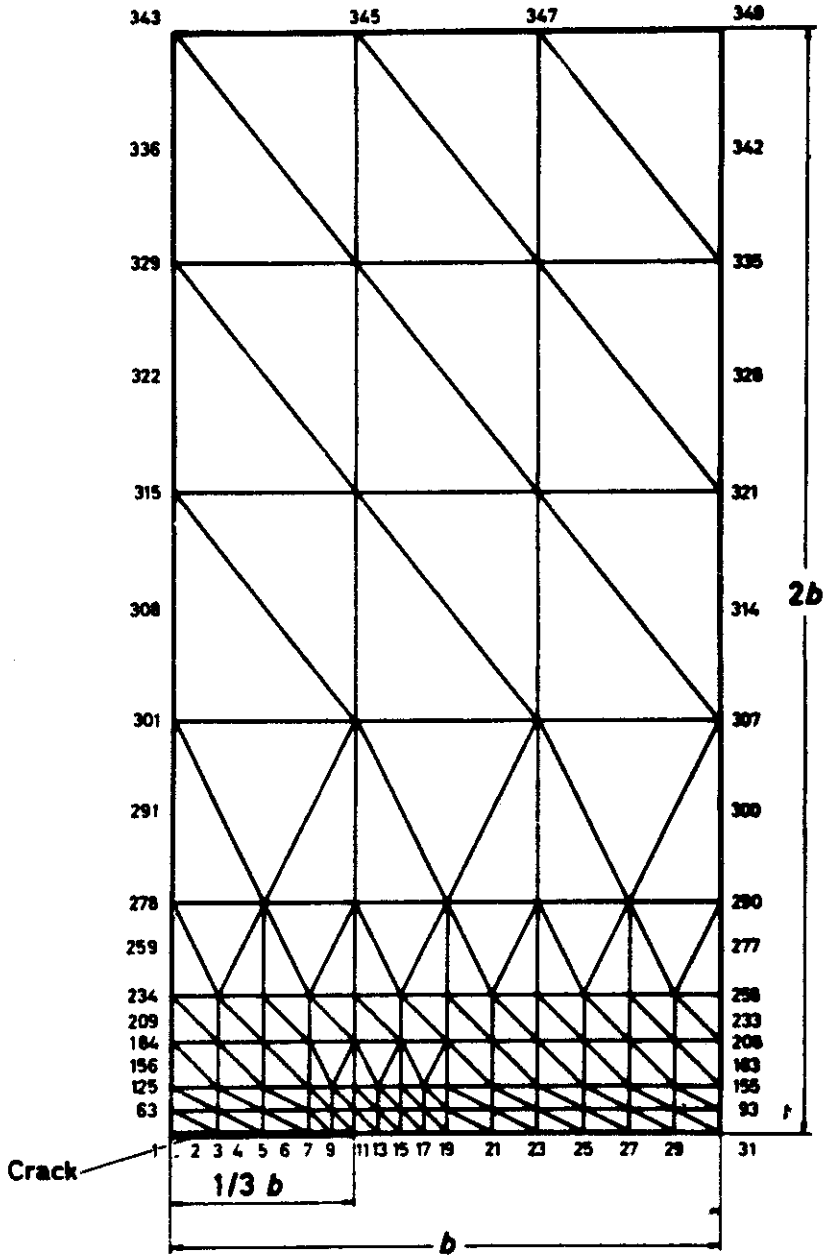

Figure 31. Idealization of Cracked Plate

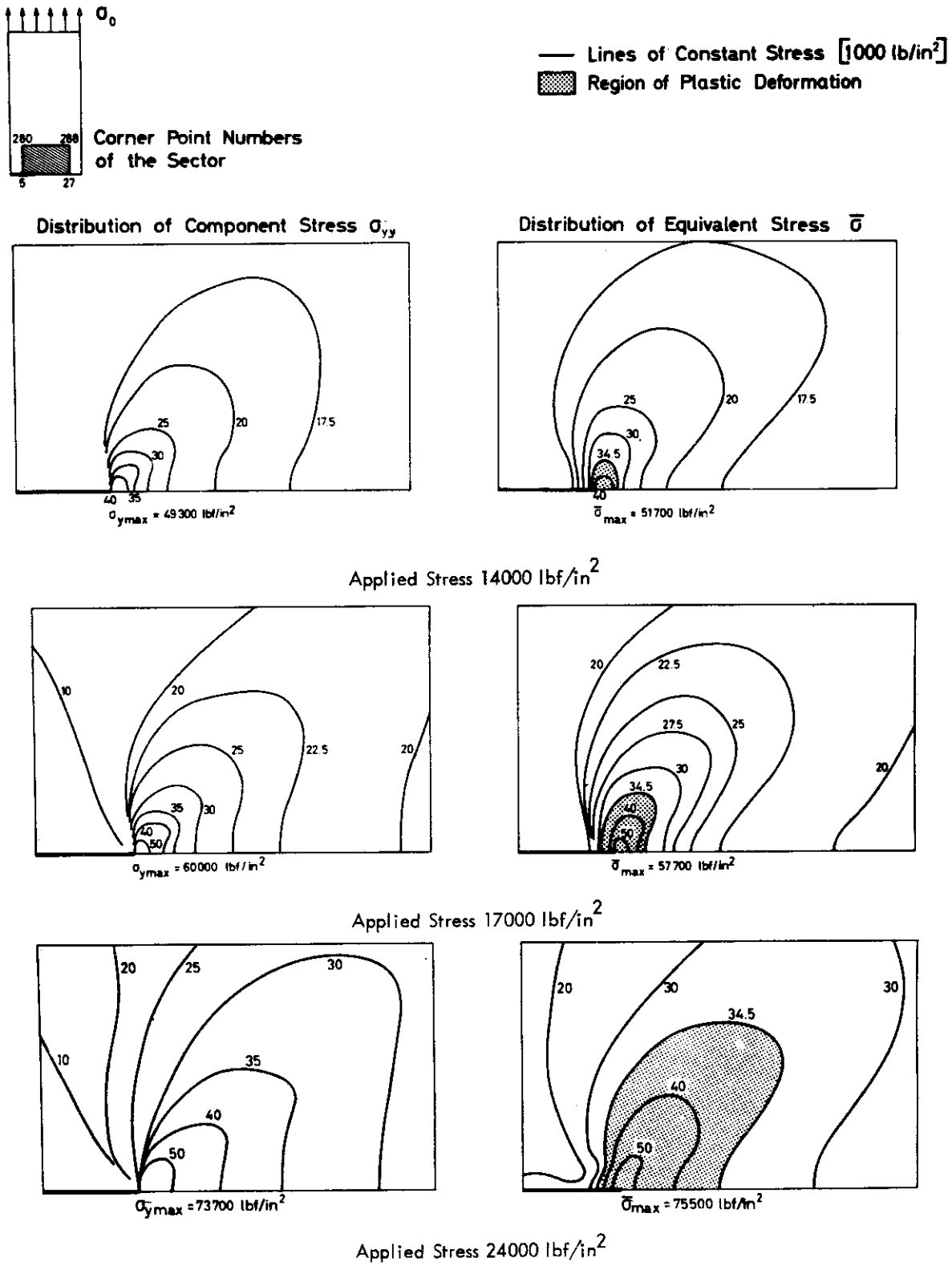

Figure 32. Plate with Crack

SECTION V

SOME ASPECTS OF LARGE DISPLACEMENT ANALYSIS

1. GENERAL CONSIDERATIONS

We presented in Reference 1 a review of the progress achieved until autumn 1965 in the application of the natural mode technique to the large displacement analysis and secondary instability effects, like snap-through, in elastic systems. Since then considerable advances have been realized at ISD and Imperial College, mainly in a new philosophical direction, involving continuously varying curvilinear elements; see Section I, Figure 6. The relevant theory is very general, but fits neatly into the ASKA scheme. Essential refinements of the large displacement analysis of Reference 1 will be discussed. These presume the natural mode technique and were evolved by Kelsey at Imperial College in 1967. Independently, they were also developed by the senior author in his lectures at U.C.L.A., and M.I.T. in 1966-67. Graduate students at I.C. working under the direction of Kelsey and at M.I.T. under the senior author applied it successfully to a number of examples. Some of the relevant theory and illustrations may be found in Reference 26. The analysis is essentially based on a consistent application of the incremental equations (V, 24, 25) of Reference 1, which we rewrite in the form

$$\mathbf{R}_{\Delta} = \mathbf{K}\,\mathbf{r}_{\Delta} = \left[\mathbf{K}_{E} + \mathbf{K}_{G}\right]\mathbf{r}_{\Delta} \qquad (183)$$

where $\mathbf{R}_{\Delta}, \mathbf{r}_{\Delta}$ are the incremental load and displacement vectors, $\mathbf{K}_{E}$ the elastic and $\mathbf{K}_{G}$ the so-called geometric stiffness of the assembled system. For the sake of simplicity, the contribution of the initial loads is ignored in Equation 183. Given $\mathbf{R}_{\Delta}(\mathbf{r}_{\Delta})$, we may derive, in general, the associated $\mathbf{r}_{\Delta}(\mathbf{R}_{\Delta})$ and establish consequently the nonlinear load-displacement relationship. At the end of any step we may determine first the natural and then the cartesian load vector $\mathbf{P}_{N}$ and $\mathbf{P}$. The important point is now that Equation 183 neglects so-called higher order terms $\mathbf{a}^{\dagger}_{N\Delta}\mathbf{P}_{N\Delta}$ in the equilibrium condition of an element. This may lead to a considerable deviation from the true load-displacement, even when the increments are small (but inevitably finite), especially in the neighbourhood of instability or near instability states; see Figure 33.

To circumvent this difficulty it is fairly evident that we must apply an iterative procedure. Consider to this purpose a typical loading and deformation step. The fundamental transformation matrix $\mathbf{a}_N$ - relating the natural or pure deformation vector ρ_N with the total displacement vector via

$$\rho_N = \mathbf{a}_N \rho \tag{184}$$

varies over any finite increment. We denote its value at the beginning and end of the step by $\mathbf{a}_{Nb}$ and $\mathbf{a}_{Ne}$ respectively. Following Equation (V, 10) of Reference 1, the equilibrium condition would be exactly satisfied, if

$$P_g = \left[\mathbf{a}_N^t P_N\right]_g \qquad \text{for the g th element} \tag{185}$$

$$R = \sum_g \mathbf{a}_g^t P_g = \sum_g \mathbf{a}_g^t \left[\mathbf{a}_N^t P_N\right]_g \qquad \text{for the complete system} \tag{186}$$

were true. Since first approximation is used in the linearized increment, Equations 185 and 186 hold only approximately. There remain, in fact unbalanced forces

$$R_u = R - \sum_g \mathbf{a}_g^t P_g \tag{187}$$

We should compute a new linearized increment based on the new geometry at e and the residual vector R_u and continue this relaxation until R_u is eliminated to any preset accuracy, e.g. 10^{-3} kg. In Equations 185, 186 and 187 the index Δ is omitted for economy in subscripts.

Clearly we can refine and accelerate the technique by allowing a second or even fourth order accuracy. To account for second order terms we rewrite Equation (V, 13) (Reference 1) for the gth element in the evident form

$$\rho_{Ng\Delta} = \frac{1}{2}\left[\mathbf{a}_{Nb} + \mathbf{a}_{Ne}\right]_g \rho_{g\Delta} \tag{188}$$

$$P_{Ng\Delta} = k_{Ng}\rho_{Ng\Delta} = \frac{1}{2} k_{Ng}\left[\mathbf{a}_{Nb} + \mathbf{a}_{Ne}\right]_g \rho_{g\Delta} \tag{189}$$

which means that the natural load vector $P_{N\Delta}$ of the elements derives from an average value $\mathbf{a}_N$ at the beginning and end of the step. In general, Equations 188 and 189 prove sufficiently accurate for a fast convergence of the iteration procedure to eliminate the unbalanced loads R_u.

However, we may account for fourth order terms and the slope of the r-R curve at the initiation and end of the current step by remembering Equation (V, 19) (Reference 1) for the definition of the geometrical stiffness via the ν modal component matrices Λ_δ where

$$\Lambda_\delta = \frac{\partial a^{\dagger}_{N\delta}}{\partial \rho} \tag{190}$$

We find for the higher approximation of the submatrix $a_{N\delta}$ of a_N (see Equation V, 8, Reference 1)

$$a_{Ng\delta} = \frac{1}{2}\left[a_{N\delta b} + a_{N\delta e}\right]_g + \frac{1}{12}\rho_g^{\dagger}\left[\Lambda_{\delta b} - \Lambda_{\delta e}\right]_g \tag{191}$$

and hence

$$\rho_{Ng\delta} = \frac{1}{2}\left[a_{N\delta b} + a_{N\delta e}\right]_{g\rho g} + \frac{1}{12}\rho_g^{\dagger}\left[\Lambda_{\delta b} - \Lambda_{\delta e}\right]_{g\rho g} \tag{192}$$

from which we derive a more accurate $P_{N\Delta}$ and so on.

In practical applications it is, in general, also necessary to account for the effect of the effect of the P_N in modifying the elastic stiffness. This is the so-called end load effect in beam elements. Its influence is described by the "natural geometrical stiffness" k_{NG} of Reference 1, which must be added to the current pure elastic stiffness k_{NE}; see Equation (V, 42) (Reference 1). The theory of continuous two- and three-dimensional systems using curvilinear triangular and tetrahedron elements, as developed in Reference 6, includes ab initio this effect.

2. EXAMPLES

We consider here two simple examples for which exact or near exact analytical results are available. The first investigates the large displacements of a cantilever beam under a transverse load R at the tip. Figures 34 and 35 reproduce the nondimensional tip deflexions, w_T/ℓ and $-u_T/\ell$. They are based on a slenderness ratio $\lambda = \ell/i = 120$ and presume a ten-element idealization. True equilibrium was assumed to be attained when $|R_u| \leq 10^{-4}$ kg. In the range $R\ell^2/EI > 1.0$ the nondimensional loading increment $R_\Delta \ell^2/EI$ was fixed at 0.1; for $R\ell^2/EI > 1.0$ the increment was increased to 0.5, although 1.0 proves equally satisfactory. The exact results are based on an infinite direct load stiffness or $\lambda = \infty$. We observe excellent agreement to which contributes the very small effect of the end load on the elastic stiffness.

The second example is mainly concerned with the post-buckling regime of a strut or beam under end load; see Figure 36. Here it is impossible to achieve a post-buckling equilibrium condition unless the above iterative method or a related technique is applied. The effect of the natural geometrical stiffness k_{NG} is, in contrast to the first example, significant. It was found that its inclusion yielded, for a ten-element idealization, a buckling load R_b to within an accuracy of six digits; the value of λ is again 120. Since the deflection is at the instability state indeterminate, it is necessary to impose a small deflection at this critical point. We may ensure this by applying a small lateral load, which is removed once the post-buckling regime is secured. Alternatively, we may prescribe for the beam a small initial curvature. The ten element idealization proves again timewise economical and accurate. The maximum deviation allowed from equilibrium was set at 10^{-3} Kg; this measure may be increased without significant loss of accuracy. For the non-dimensional loading increments $R_\Delta \ell^2/EI$, we chose over most of the range the value of 0.5. However, prior to reaching the theoretical buckling load R_b this was first reduced to 0.1 and then to 0.01 and 0.005. In the post-buckling regime the value was first increased to 0.01, then to 0.1 resp. 0.2, the ultimate value being once more 0.5. We restrict our considerations to a beam with an initial curvature of

$$w_o/\ell = 0.001(1 - \cos \pi x/\ell) \tag{193}$$

Figure 36 reproduces some of the results for the tip deflection w_T/ℓ and compares them with the von Mises theory (valid for small deflections prior and subsequent to buckling) and the Timoshenko theory (valid for large deflections). Excellent agreement is observed, which also holds for high values of R/R_b not shown in the diagram. If initial curvature is varied, we find in accordance with analysis that the effect is pronounced prior to and just beyond the theoretical buckling state, but once R/R_b is large its influence becomes small.

When an initial transverse load is chosen, instead of the preset curvature, the computations are equally straightforward.

The theory discussed here in broad terms has been extended to snap-through problems of arches, spherical caps and general shells of revolution. It is found that, with increasing complexity of the problems, the new approach developed in Reference 6 proves more fruitful.

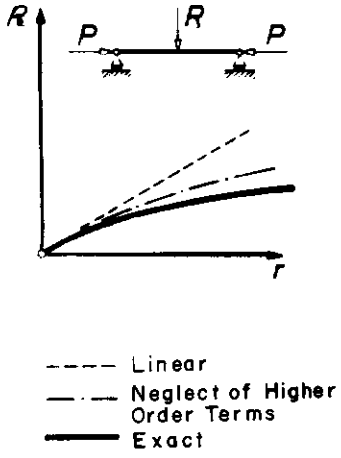

Figure 33. Nonlinear Behaviour of System-Softening Effect with Large Displacements (Due to Applied Compression Load P on Beam)

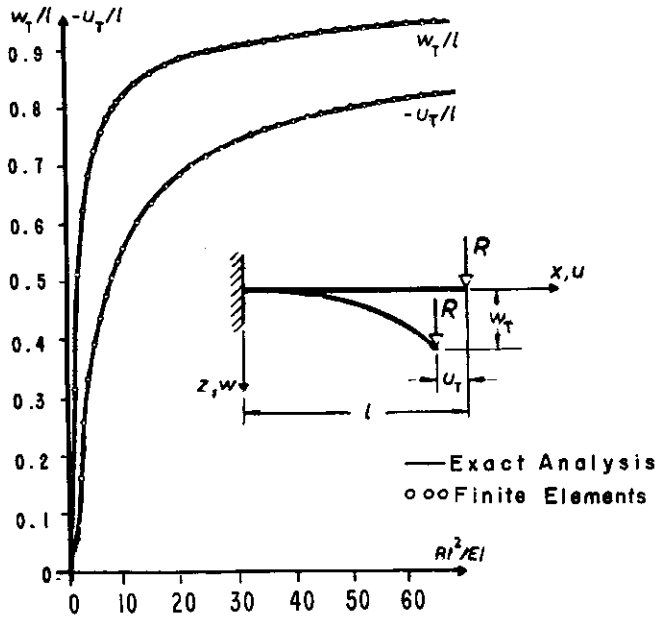

Figure 34. Tip Displacements versus

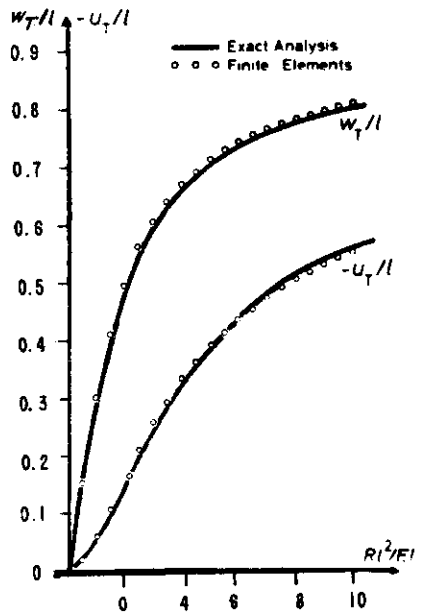

Figure 35. Cantilever Beam under Transverse Load

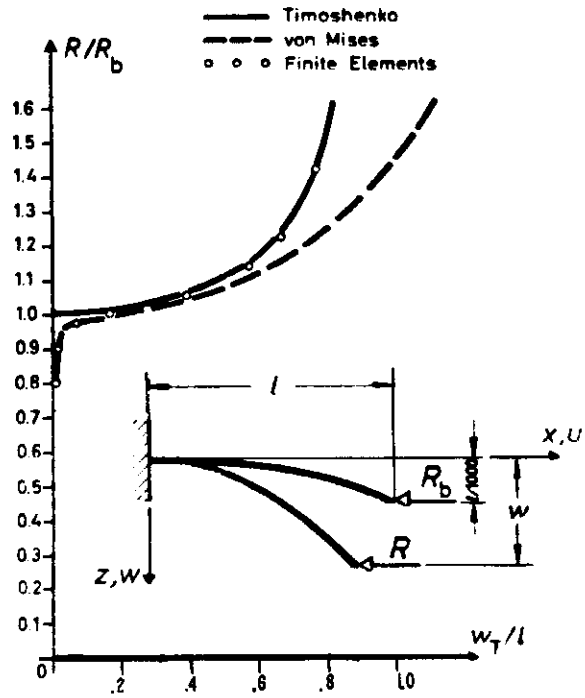

Figure 36. Beam with Initial Curvature

SECTION VI

REFERENCES

1. Argyris, J. H., "Continua and Discontinua," Opening Paper to the Air Force Conference on Matrix Methods in Structural Mechanics at Wright-Patterson Air Force Base, Dayton, Ohio, 26-28 October, 1965. Proceedings, December 1966.

2. Argyris, J. H., "The Computer Shapes the Theory," Lecture to the Royal Aeronautical Society, 19 May, 1965 to be published in The Aeronautical Journal of the Royal Aeronautical Society.

3. Argyris, J. H., Fried, L, "The LUMINA Element for the Matrix Displacement Method," The Aeronautical Journal of the R.Ae.S., Vol. 72, No. 690, pp. 514-517, June 1968.

4. Argyris, J. H., Fried, L, Scharpf, D. W., "The HERMES Element for the Matrix Displacement Method," The Aeronautical Journal of the R.Ae. S., Vol. 72, No. 691, pp. 613-617, July 1968.

5. Argyris, J. H., Fried, L, Scharpf, D. W., "The TET 20 and TEA Elements for the Matrix Displacement Method," The Aeronautical Journal of the R.Ae.S., Vol. 72, No. 691, pp. 618-623, July 1968.

6. Argyris, J. H., Scharpf, D. W., "Curved Triangular and Tetrahedron Elements for Large Displacement Analysis," ISD Report No. 51. To be published in The Aeronautical Journal of the R.Ae.S.

7. Argyris, J. H., Redshaw, S. C., "Three-Dimensional Analysis of Two Arch Dams by a Finite Element Method, "Part II, Paper presented at the Symposium on Arch Dams, Institute of Civil Engineers, March 18-20, 1968.

8. Argyris, J. H., Spooner, J. B., Weber, J., "Berechnung räumlicher Spannungsverteilungen in Staudämmen nach der Matrizenverschiebungsmethode," Ingenieur Archiv, 36. Band, 5. Heft, S.320-334, 1968.

9. Mareczek, G., Scharpf, D. W., Three-Dimensional Analysis of a Heated Turbine Vane, A Finite Element Application Using the Displacement Method, ISD Report No. 52, July 1968. To be published.

10. Mareczek, G., Scharpf, D. W., Three-Dimensional Analysis of a Pretwisted Impeller Blade by Means of ASKA, ISD Report No. 53, July 1968. To be published.

11. Knapp, H., Scharpf, D. W., Three-Dimensional Analysis of a Heated Turbine Vane Using LUMINA and HERMES Elements, ISD Report No. 54, 1968. To be published.

12. Argyris, J. H., Fried, L, Scharpf, D. W., "The TUBA Family of Elements for the Matrix Displacement Method," The Aeronautical Journal of the R.Ae.S., Vol .72, No. 692, August 1968.

13. Argyris, J. H., Buck, K. E., "A Sequel to the TUBA Family of Plate Elements," ISD Report No. 55, July 1968. To be published in The Aeronautical Journal of the R.Ae.S.

14. Argyris, J. H., Fried, L, The PUBA Family of Plate Elements for the Matrix Displacement Method, ISD Report No. 56, August 1968. To be published in The Aeronautical Journal of the R.Ae.S.

REFERENCES (CONT)

15. Bazeley, G. P., Cheung, Y. K., Irons, B. M., Zienkiewicz, O. C., "Triangular Elements in Plate Bending - Conforming and Non-Conforming Solutions," Proceedings of the First Conference on Matrix Methods in Structural Mechanics, Wright Patterson AFB, Dayton, Ohio, October 1965.

16. Clough, R. W., Tocher, J. L., "Finite Element Stiffness Matrices for Analysis of Plate Bending," Proceedings of the First Conference on Matrix Methods in Structural Mechanics, Wright Patterson AFB, Dayton, Ohio, October 1965.

17. De Veubeke, Fraeijs, B., "Bending and Stretching of Plates - Special Models for Upper and Lower Bounds," Proceedings of the first Conference on Matrix Methods in Structural Mechanics, Wright Patterson AFB, Dayton, Ohio, October 1965.

18. Argyris, J. H., Bosshard, W., Fried, I., Hilber, H. M., A Fully Compatible Plate Bending Element, ISD Report No. 42, December 1965.

19. Argyris, J. H., Scharpf, D. W., "The SHEBA Family of Shell Elements for the Matrix Displacement Method," The Aeronautical Journal of the R.Ae.S., Vol. 72, No. 694, October 1968.

20. Argyris, J. H., Buck, K. E., Scharpf, D. W., "Matrix Displacement Analysis of Plates and Shells, Prolegomena to a General Theory," Part II. To be published in Ingenieur Archiv.

21. Bogner, F. K., Fox, R. L., Schmit, L. A., Jr., "The Generation of Interelement, Compatible Stiffness and Mass Matrices by the Use of Interpolation Formulas," Proceedings of the First Conference on Matrix Methods in Structural Mechanics, AFB, Dayton, Ohio, October 1965.

22. Pestel, E., "Dynamic Stiffness Matrix Formulation by Means of Hermitian Polynomials," Proceedings of the First Conference on Matrix Methods in Structural Mechanics, AFB, Dayton, Ohio, October 1965.

23. Argyris, J. H., Scharpf, D. W., Spooner, J. B., "Die elastoplastische Berechnung von allgemeinen Tragwerken und Kontinua," Ingenieur Archiv, 1969, Heft 1.

24. Scharpf, D. W., "Konvergenz-Kriterien für elastoplastische Untersuchungen," ISD Report 1966, and Dr. Ing.-Thesis to be published at the University of Stuttgart, 1968.

25. Argyris, J. H., Scharpf, D. W., "Elastoplastic Analysis of Arbitrary Systems." To be published in The Aeronautical Quarterly of the R. Ae.S.

26. Saadetian, H. G., "The Finite Element Matrix Analysis of a Beam in the Buckled and Post-Buckled Range," M. Sc. (Eng.) Thesis, University of London, October 1967.

27. Argyris, J. H., Buck, K. E., Fuchs, G. von, Hilber, H. M., Schrem, E., Sörensen, M., "Automatic System for Kinematic Analysis" - ASKA, ISD Report No. 57, new edition, November 1968.

REFERENCES (CONT)

28. Scharpf, D. W., Fried, I., "A Computational Procedure for Gradient Iterative Techniques in the Finite Element Method," Lecture delivered at EUROMECH 11 Conference, Stuttgart, April 8-10, 1968.

29. Argyris, J. H., Scharpf, D. W., "A Computational Procedure for Gradient Iterative Techniques in the Finite Element Method," ISD Report No. 58; to be published in Ingenieur Archiv.

30. Dunne, P. C., "Complete Polynomial Displacement Fields for Finite Element Methods," The Aeronautical Journal of the R.Ae.S., Vol. 72, No. 687, pp. 245-246, March 1968.

31. Gol'denveizer, A. L., Theory of Elastic Thin Shells, Pergamon Press, 1961.

32. Kraus, H., Thin Elastic Shells, John Wiley and Sons; London, 1967.

33. Koiter, W. T., "A Consistent First Approximation in The General Theory of Thin Elastic Shells, " Proceedings of the Symposium on the Theory of Thin Elastic Shells, IUTAM, Delft, pp. 12-33, North-Holland, Amsterdam, 1960.

34. Sanders, J. L., An Improved First Approximation Theory for Thin Shells, NASA, T. R., R-24, 1959.

35. Reissner, E., "On the Form of Variationally Derived Shell Equations," Journal of Applied Mechanics, Vol. 31, pp. 233-238, 1964.

36. Argyris, J. H., "Elastoplastic Matrix Displacement Analysis of Three-Dimensional Continua," Journal of the Royal Aeronautical Society, Vol. 69, No. 657, pp. 633-636, September 1965.

37. Morley, L. S. D., Skew Plates and Structures, Pergamon Press, Oxford, 1963.